# Copper-catalyzed enantioselective conjugate addition of Grignard reagent to non-activated acceptors

Yan, Xingchen

# Chapter 3: Mechanistic studies on Lewis acid enabled copper-catalyzed enantioselective conjugate addition of Grignards to $\alpha,\beta$-unsaturated carboxamides

The presence of a strong LA together with chiral Cu(I)-catalyst and highly reactive Grignard reagents in the catalytic system developed in the chapter 2 makes for a complex system. Here, we studied the mechanism which revealed the fate of the Lewis acid in each elementary step of this reaction. Based on theses studies the most likely catalytic cycle for the copper-catalyzed asymmetric conjugate addition of Grignards to $\alpha,\beta$-unsaturated carboxamides is proposed.

Part of this chapter has been published:

M. Rodríguez-Fernández, X. Yan, J. F. Collados, P. B. White, S. R. Harutyunyan, *J. Am. Chem. Soc.* **2017**, *139*, 14224–14231.

## 3.1 Introduction

It is generally assumed that the mechanism of the Cu-catalyzed enantioselective CA of organometallic compounds follows similar principles as proposed for the non-catalytic organocuprate addition. The latter proceeds through reversible formation of a copper-olefin $\pi$-complex, involving d,$\pi^*$ back-donation, followed by a formal oxidative addition to the $\beta$-carbon leading to a $d^8$ copper(III) intermediate and, finally, reductive elimination to form the enolate involving an oxidative addition-reductive elimination pathway (Scheme 1).[1-16]

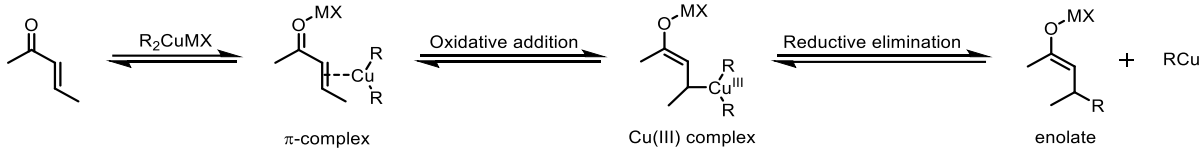


**Scheme 1:** proposed mechanistic pathway for the stoichiometric 1,4-addition of organocuprates.

In 2006, Feringa *et. al.* performed a detailed mechanistic study of the copper-catalyzed CA of Grignard reagents by combining spectroscopic studies, kinetic analysis, and screening of reaction parameters.[17] They found that there is a rapid equilibration for the chiral Cu-catalyst to form either a mononuclear (**3** and **4**) or a dinuclear (**1** and **2**) complex, depending on the solvent employed (Scheme 2).[18] The preparation of the bromide complex from CuX and ligand **L** (**L1** or **L2**) using ethereal ($Et_2O$, MTBE) or halogenated (DCM, $CHCl_3$) solvents led to the dinuclear structures **1** or **2**. In contrast, the mixture of CuBr and ligand **L** (**L1** or **L2**) in $CH_3CN$ or MeOH led to the formation and precipitation of the mononuclear complex **3** or **4**. This mononuclear Cu-complex **3** or **4** can also be prepared by dissolving the dinuclear complex **1** or **2** in $CH_3CN$. In contrast to the dinuclear complex **1** or **2**, the mononuclear complex **3** or **4** is insoluble in $Et_2O$ and MTBE. However, in halogenated solvents, such as DCM or $CHCl_3$, **3** or **4** dissolves readily, yielding the dinuclear complex **1** or **2**.

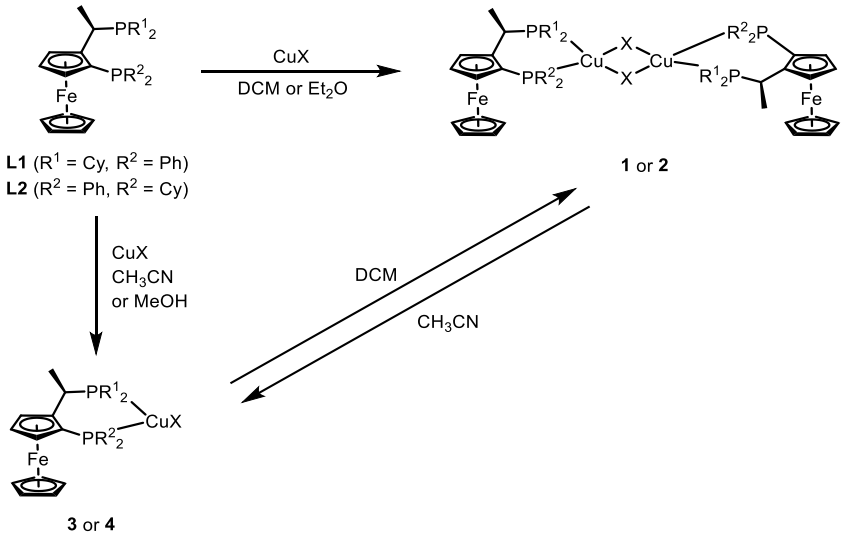


**Scheme 2:** equilibration between the mononuclear and the dinuclear complex.

Keeping in mind that ACA reactions with Grignard reagents typically make use of ethereal ($Et_2O$, MTBE) or halogenated (DCM, $CHCl_3$) solvents, the dinuclear complex (**1** and **2**) will be formed first. Upon addition of MeMgBr to the solution of the dinuclear complex, transmetallation occurs resulting in mononuclear complex **A**, accompanied by the formation of traces of species **B** (Scheme 3). In contrast, when MeLi or $Me_2Mg$ are used rather than Grignard reagents, species **C** is formed instead.

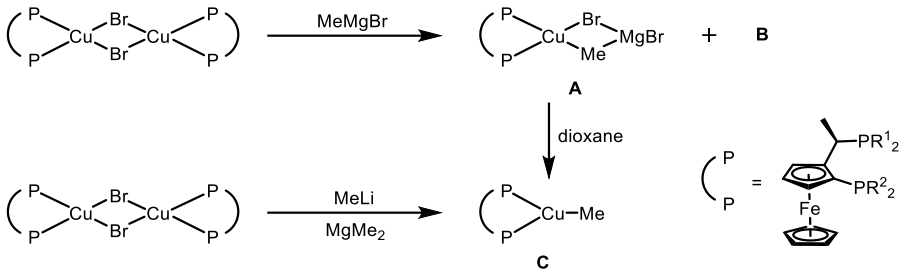


**Scheme 3:** transmetallation of the catalyst with MeMgBr or MeLi to give rise to species **A**, **B** and **C**.

The same authors also found that addition of an equimolar amount of Michael acceptor substrates to either species **A** or **C** led to the formation of the conjugate addition products. The reaction with species **A** proceeded with excellent conversion and enantioselectivity whereas with species **C** lower conversion and *ee* was observed. Taking into account that species **C** can be formed by either addition of $Me_2Mg$ to the dinuclear complex or of dioxane to species **A**, the data correlates well with the low conversion and enantioselectivity obtained in the catalytic reactions performed with $Me_2Mg$ and with MeMgBr in combination with dioxane as an additive (dioxane is commonly is used as a reagent to prepare $R_2Mg$ from RMgBr by binding to $MgBr_2$). Thus, the generation of species **A**, rather than **C**, is essential to obtain high levels of regio- and enantioselectivity in the catalytic CA of Grignard reagents to *α,β*-unsaturated carbonyl compounds. Species **B** was considered a side product accompanying the formation of species **A** and **C** and its structure remained unknown until the work described in this thesis (see below).

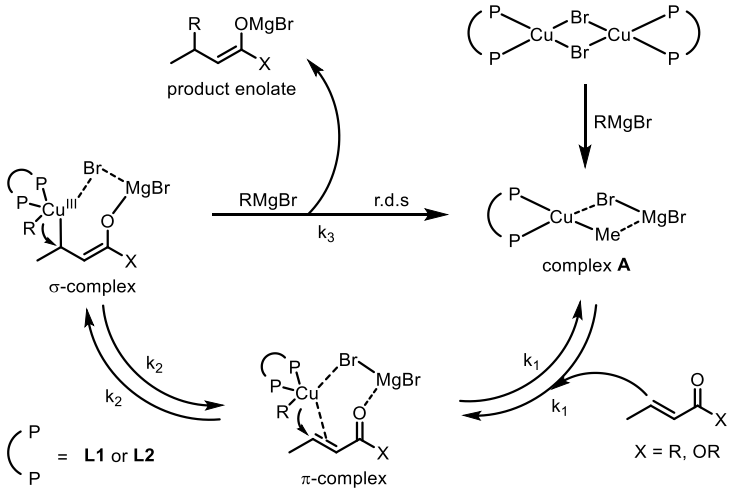


**Scheme 4:** proposed catalytic cycle for the CA addition of Grignard reagents to *α,β*-unsaturated carbonyl compounds.

Based on speciation analysis and also kinetic studies a catalytic cycle was proposed for the ACA of Grignard reagents to *α*,*β*-unsaturated carbonyl compounds (Scheme 4). In this proposal the first step in the catalytic cycle is initiated by the transmetallation between the dimeric precatalyst and RMgBr to form the catalytically active complex **A**. Then the copper in complex **A** binds to the double bond of the substrate to form the *π*-complex with an additional interaction of $Mg^{2+}$ with the oxygen atom of the carbonyl moiety. $Mg^{2+}$ is important for the reaction because removing $Mg^{2+}$ from the system leads to the formation of species **C**, thus giving the products with lower conversion and *ee*. The formation of a *π*-complex is possibly followed by intramolecular rearrangement to a Cu(III)-intermediate where copper forms a *σ*-bond with the *β*-carbon of the enone (or enoate). The combination of Grignard reagent, diphosphine ligand, as well as the halogen still bound to the copper, provides donor ligands (electrons) to this formal organocopper species, that consequently has the reactivity and electronic properties of cuprate types of structures. In addition to inducing increased reactivity, these donor ligands also ensure the necessary geometry of the *σ*-complex and afford excellent regio- and stereocontrol in ACA reactions. This *σ*-complex is in fast equilibrium with the *π*-complex, and the equilibrium constant between both complexes depends on the stability of the Cu(III)-intermediate. This fast equilibrium can cause the isomerization of the substrate from the *cis*-configuration to the more stable *trans*-configuration. The final step is the rate-limiting, reductive elimination step to generate the product enolate and recover the catalytically active complex **A**. The results demonstrate that the rate of the reaction depends on all the reacting components, and is first order in the catalyst and second order in the Grignard reagent.

In principle, the mechanism of LA enabled Cu-catalyzed ACA of Grignards to *α*,*β*-unsaturated carboxamides should be similar to the Cu-catalyzed ACA of Grignard reagents to *α*,*β*-unsaturated carbonyl compounds. However, the necessary presence of LA to accomplish enantioselective CA to *α*,*β*-unsaturated carboxamides adds another level of mechanistic complexity. LA additives have been known for decades to accelerate the CA of organometallics to various *α*,*β*-unsaturated carbonyl derivatives.[19] In particular, the use of very weak TMSCl became common practice in CA of various hard organometallics.[19-25] In contrast, relatively strong LAs, such as $BF_3{\cdot}Et_2O$, have been used only in CA of stoichiometric organocopper reagents.[19,26-28] In our case, the presence of a strong LA together with only few percent of chiral Cu(I)-catalyst and highly reactive Grignard reagents makes for a complex system. Therefore, we performed mechanistic study to gain a deeper understanding on the role of LA in our catalytic system.

## 3.2 Results and discussions

The outcome of the reaction depends critically not only on the relative rates of the desired catalyzed and the undesired non-catalyzed pathways but also on those of several competing processes (Scheme 5). We proposed a new catalytic cycle for Cu-catalyzed ACA of Grignards to *α*,*β*-unsaturated carboxamides involving LA based on the mechanistic studies (Scheme 6). We expect the catalytic cycle to be initiated by the formation of species **6** through transmetallation of chiral catalyst **1** by Grignard reagents.


**Scheme 5:** undesired reaction pathways in the CA of Grignard reagents to $\alpha,\beta$-unsaturated carboxamides in the presence of LA followed by $^{1}$H NMR spectroscopy in $CD_2Cl_2$ at −80 °C.

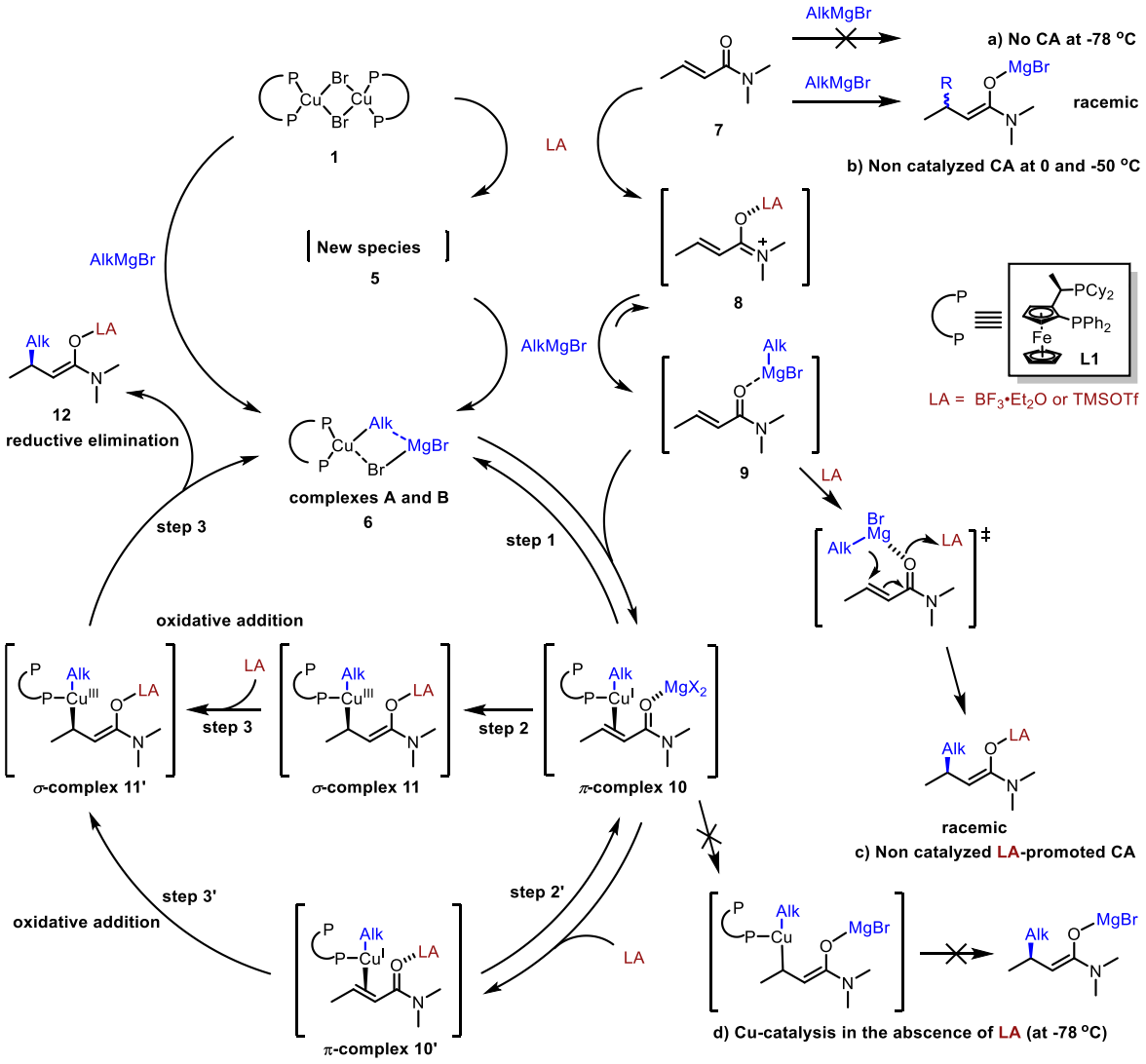


**Scheme 6:** proposed catalytic cycle for the LA enabled ACA addition of Grignard reagents to carboxamide.

We prepared species **6** by addition of MeMgBr to chiral catalyst **1** and analyzed it by $^{1}$H and $^{31}$P NMR spectroscopy. A 3.0 M MeMgBr solution in $Et_2O$ (20 $\mu$L, 0.06 mmol) was added to a solution of catalyst **1** (11 mg, 0.015 mmol) in $CD_2Cl_2$ (0.6 mL) in a dry NMR tube at −78 °C and the resulting mixture was immediately measured by $^{1}$H and $^{31}$P NMR spectroscopy at −80 °C. Two different transmetallated complexes **A** and **B** (species **6**) were detected as expected (Figures 1 and 2). Both species present methyl moieties coupled with both phosphines with the same pattern in the $^{1}$H-$^{31}$P HMBC spectrum (Figure 3). Species **A** and **B** conform to the previously reported species **A** and **B** (Scheme 3) in the mechanistic study on the CA addition of Grignard Reagents to $\alpha,\beta$-unsaturated carbonyl compounds.[17] We have redefined the structure of species **6** based on these data: species **B**: −0.28 ppm, dd, Cu*Me* in $^{1}$H NMR; 14.8 (d, $J$ = 155.5 Hz), −18.0 (d, $J$ = 155.5 Hz) in $^{31}$P NMR and species **A**: −0.37 ppm, dd, Cu*Me* in $^{1}$H NMR; 7.5 (d, $J$ = 144.3 Hz), −26.4 (d, $J$ = 144.3 Hz) in $^{31}$P NMR. For both

species the integration indicates that only one methyl group is bound to the copper (based on the 1:1 ratio measured by comparison of the Me signal with signals from the ferrocene). For these reasons both species **A** and **B** are assumed to be the two possible diastereoisomers of the transmetallated species **6**. One can imagine that transmetallation of enantiopure chiral Cu-complex **1** proceeds with the formation of two diastereoisomers (orientation of the Me group with respect to the ferrocenyl ligand in the Cu-bound complex) where species **A** is the major and species **B** the minor one**.** The catalytic activity of species **A** and **B** is identical as well.

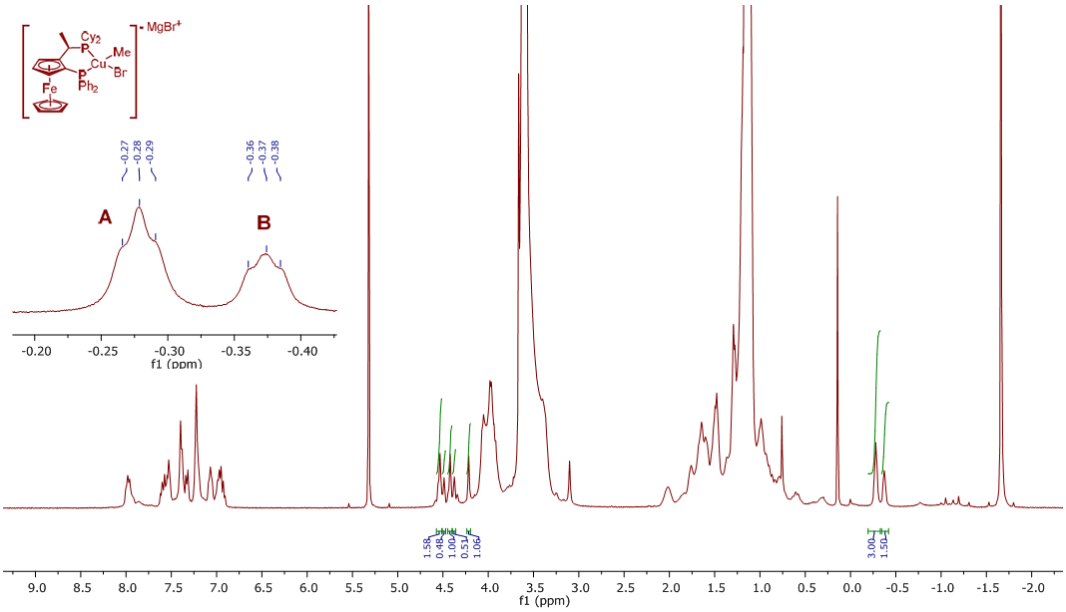


**Figure 1:** $^{1}$H NMR spectrum of the transmetallated species **6**.

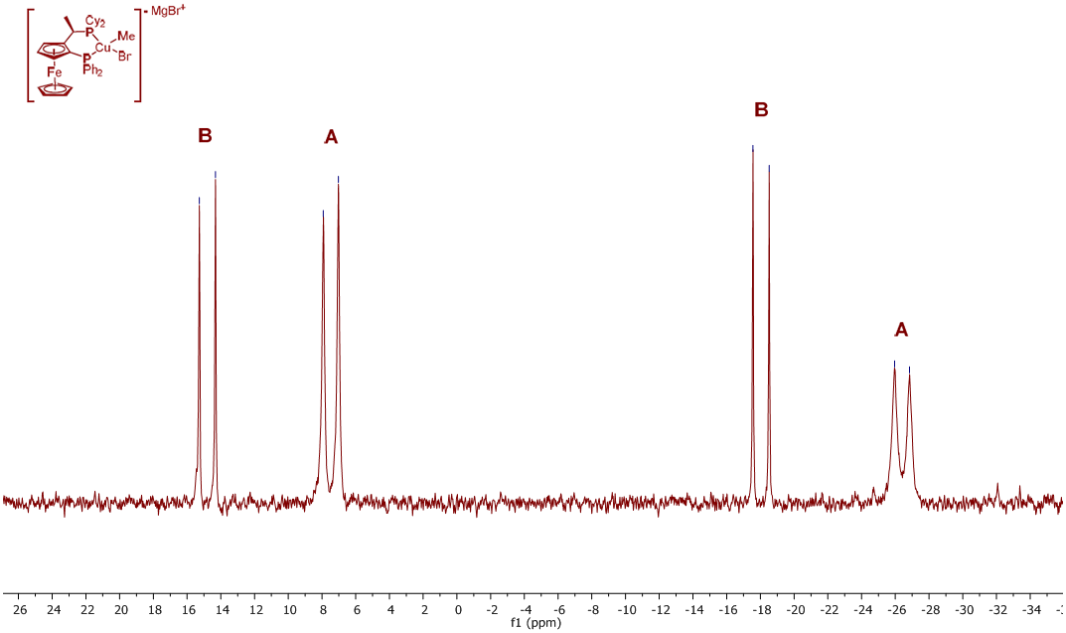


**Figure 2:** $^{31}$P NMR spectrum of the transmetallated species **6**.

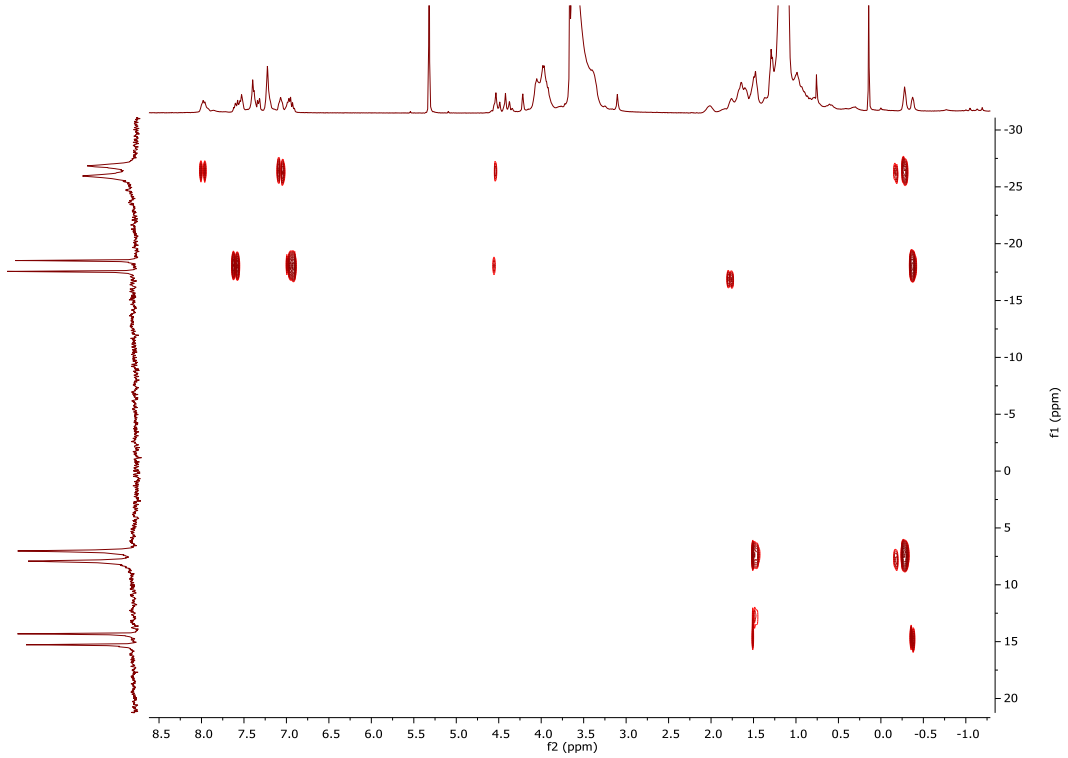


**Figure 3:** $^{1}H$-$^{31}P$ HMBC spectrum of the transmetallated species **6**. Similar pattern of coupling with the phosphines is observed for both species.

However, the chiral ligand **L1**, reversibly bound to copper, is Lewis basic, and thus a strong LA competes with copper for binding to **L1**, potentially destroying the chiral catalyst **1** (Scheme 5). This was confirmed by a control experiment that saw the formation of a mixture of unidentified species lacking bidentate coordination to copper (singlets versus doublets in $^{31}P$ NMR) upon addition of either LA to chiral copper complex **L1**-CuBr (Figure 4). Remarkably though, addition of MeMgBr to this mixture resulted in an immediate recovery of either the **L1**-CuBr or the transmetallated copper complex **6**, depending on the remaining amount of Grignard reagent in the media. Similarly, adding an excess of LA to the transmetallated copper complex did not affect its structure. Even when adding copper salt and Grignard after combining LA with **L1**, species **6** is formed, demonstrating its remarkable formation rate and stability.

This can be proved by a set of experiments we carried out. Complex **L1**-CuBr (5.9 mg, 0.08 mmol) was dissolved in $CD_2Cl_2$ (0.6 mL) in a dry NMR tube under a $N_2$ atmosphere and cooled down to −78 °C. TMSOTf (15 $\mu$L, 0.08 mmol) or $BF_3{\cdot}Et_2O$ (10 $\mu$L, 0.08 mmol) were added to the complex and the resulting mixture was analyzed by $^{1}H$ and $^{31}P$ NMR spectroscopy at −60 °C. Complex **L1**-CuBr (doublets, Figure 4b) disappeared in both cases and unidentified phosphorus containing species were formed: singlets at 27.1 and 4.4 ppm; with TMSOTf (Figure 4c) , and singlets at 31.9, 0.5 and −0.3 ppm; with $BF_3{\cdot}Et_2O$ (Figure 4d). Observing phosphorus signals as singlets instead of the initial doublets indicates detachment of, at least, one of the phosphine moieties of the complex **L1**-CuBr. Formation of new **L1**-CuBr complex with monodentate instead of bidentate coordination cannot be excluded either. After cooling down again to −78 °C, a 3 M MeMgBr solution in $Et_2O$ (67 $\mu$L, 0.2 mmol) was added and the mixture was analyzed by $^{1}H$ and $^{31}P$ NMR spectroscopy at

−60 °C. Importantly the transmetallated **L1**-CuBr species **6** was observed in both cases, although in the case of TMSOTf only isomer **A** (Figure 4e) and in the case of $BF_3{\cdot}Et_2O$ only isomer **B** among other signals (Figure 4f). Similarly, the addition of TMSOTf or $BF_3{\cdot}Et_2O$ to the transmetallated species **6** (Figure 4b) does not change the structure of the complex and the same NMR spectra were obtained (not depicted).

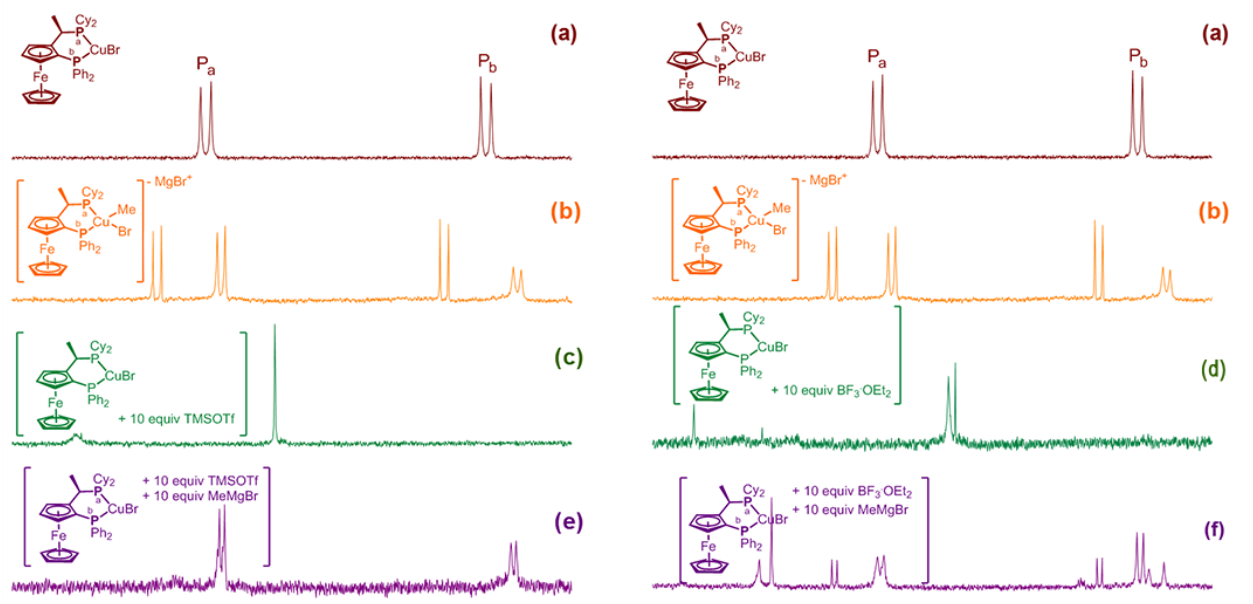


**Figure 4:** $^{31}P$ NMR spectra of combinations of **L1**-CuBr, MeMgBr and LA. Left column: from top to bottom the panels show the spectra of (a) the L1-CuBr complex, (b) the transmetallated species **6** (with **A** and **B** diastereoisomers), (c) **L1**-CuBr after adding 10 equiv. of TMSOTf, (e) the result of adding 10 equiv. of MeMgBr to (c) leading to the formation of species **A**. Right column: same as left column, but using $BF_3{\cdot}Et_2O$ instead of TMSOTf. (a) the **L1**-CuBr complex, (b) the transmetallated species **5** (with **A** and **B** diastereoisomers), (d) **L1**-CuBr after adding 10 equiv. of $BF_3{\cdot}Et_2O$, (f) the result of adding 10 equiv. of MeMgBr to (d) leading to the formation of species **A** and **L1**-CuBr together with decomposed complex peaks from (d).

Apart from the undesired reaction between the LA and the **L1**-CuBr complex another potential problem in this catalytic system is the reaction between the LA and the Grignard reagent: transmetallation of the LA by the Grignard reagent can deplete both components, as was confirmed by NMR spectroscopy. An equimolar mixture of MeMgBr solution in $Et_2O$ (33 $\mu$L, 0.1 mmol) and $BF_3{\cdot}Et_2O$ (12 $\mu$L, 0.1 mmol) in $CD_2Cl_2$ (0.6 mL) was prepared in a dry NMR tube under $N_2$ atmosphere at −78 °C and measured by NMR spectroscopy at −80 °C. Formation of $Me_4BMgBr$ (−0.74 ppm, q, $J$ = 3.7 Hz in $^1H$ NMR, −19.8 ppm, m, $J$ = 3.7 Hz in $^{11}B$ NMR) was immediately detected at −80 °C (Figures 5 and 6). Likewise, formation of $Me_4Si$ (−0.08 ppm in $^1H$ NMR, Figure 7) was detected by $^1H$ NMR at −60 °C when MeMgBr (solution 3 M in $Et_2O$, 33 $\mu$L, 0.1 mmol) was added to a solution containing TMSOTf (18 $\mu$L, 0.1 mmol) in $CD_2Cl_2$ (0.6 mL).

Thus, NMR guided control experiments confirmed that in the absence of unsaturated carboxamide substrate or **L1**-CuBr complex, all pathways indicated in Scheme 5 can occur. Fortunately, the excellent results observed for our system constitute evidence that all these processes are outcompeted by the catalyzed reaction.

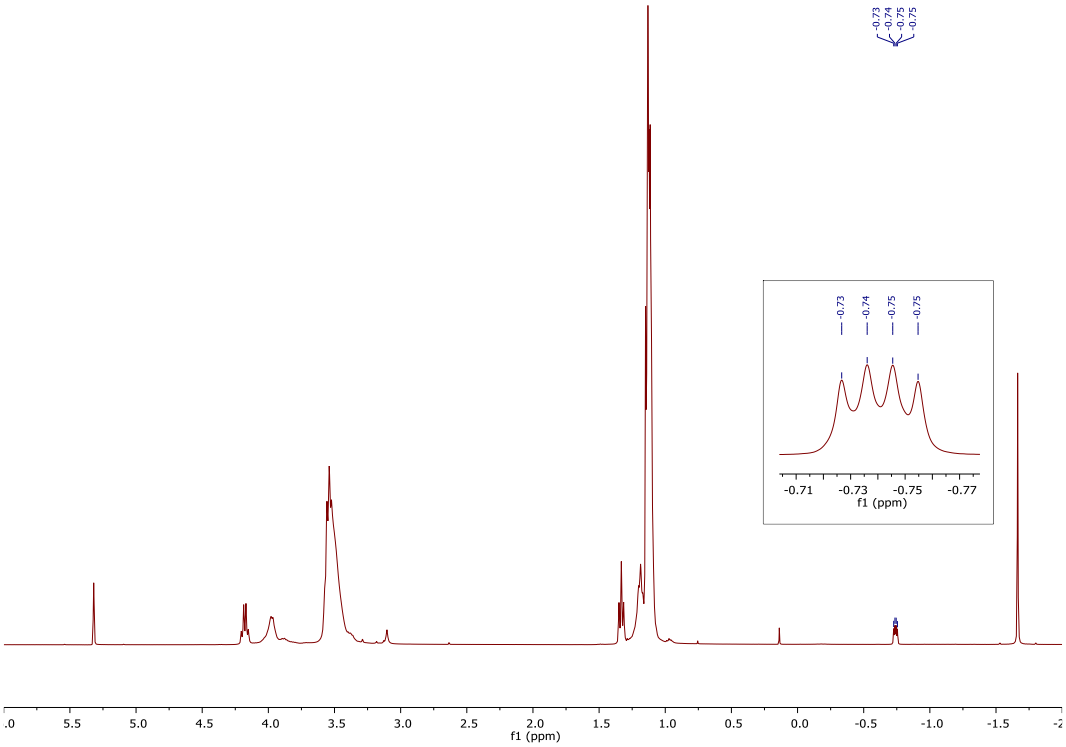


**Figure 5:** $^{1}H$ NMR spectrum of the equimolar mixture of MeMgBr and $BF_3{\cdot}Et_2O$ in $CD_2Cl_2$.

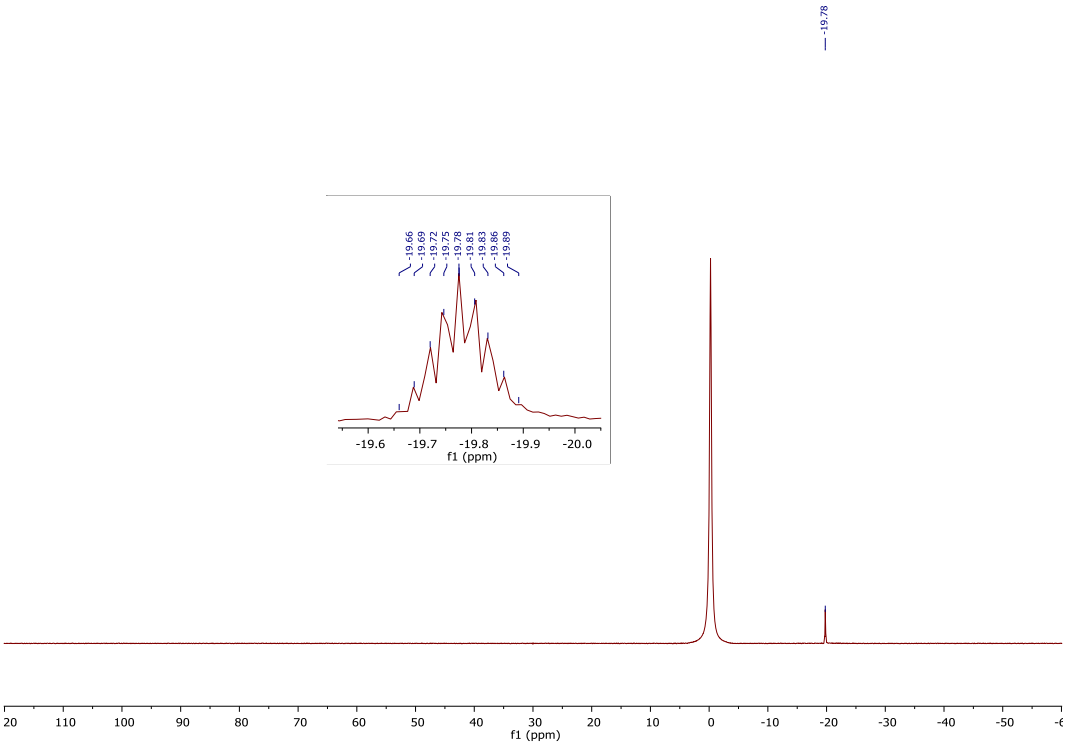


**Figure 6:** $^{11}B$ NMR spectrum of the equimolar mixture of MeMgBr and $BF_3{\cdot}Et_2O$ in $CD_2Cl_2$.

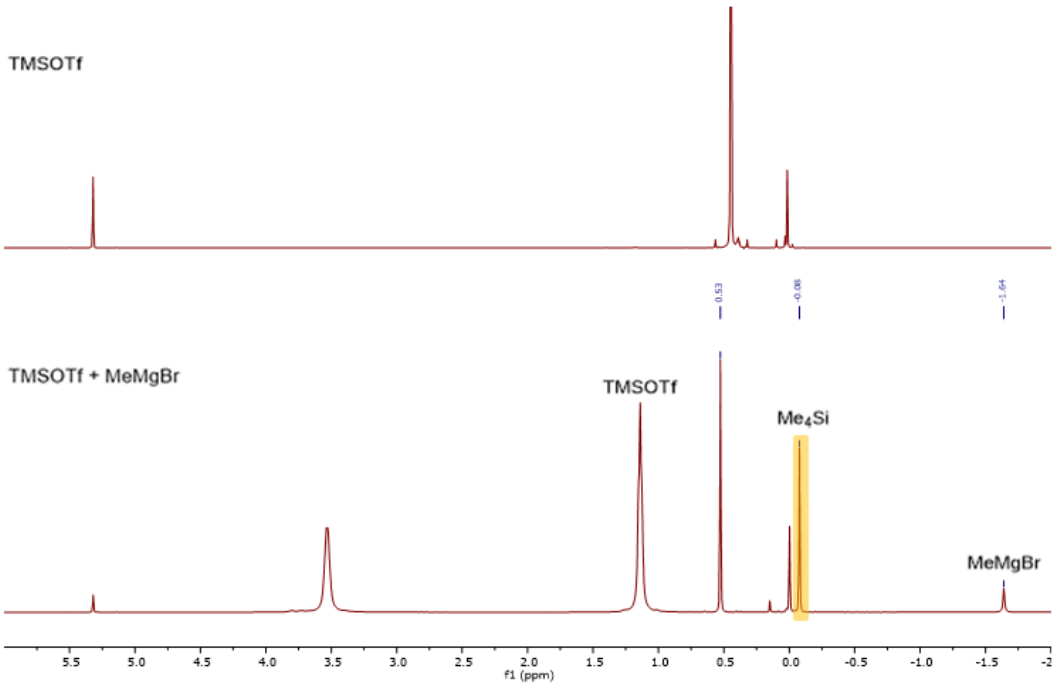


**Figure 7:** $^{1}H$ NMR spectrum of TMSOTf (top) and the equimolar mixture of MeMgBr and TMSOTf in $CD_2Cl_2$ (bottom). Appearance of a new peak of $Me_4Si$ was immediately detected (highlighted).

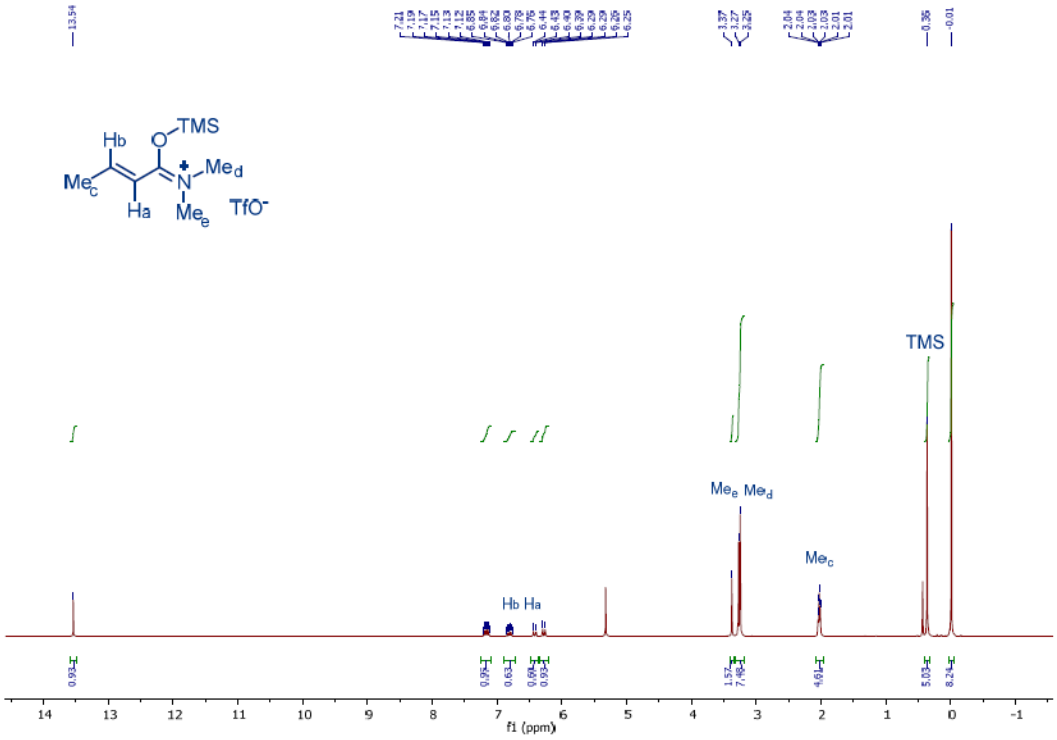


**Figure 8:** $^{1}H$ NMR spectrum of the equimolar mixture of carboxamide **7** and TMSOTf.

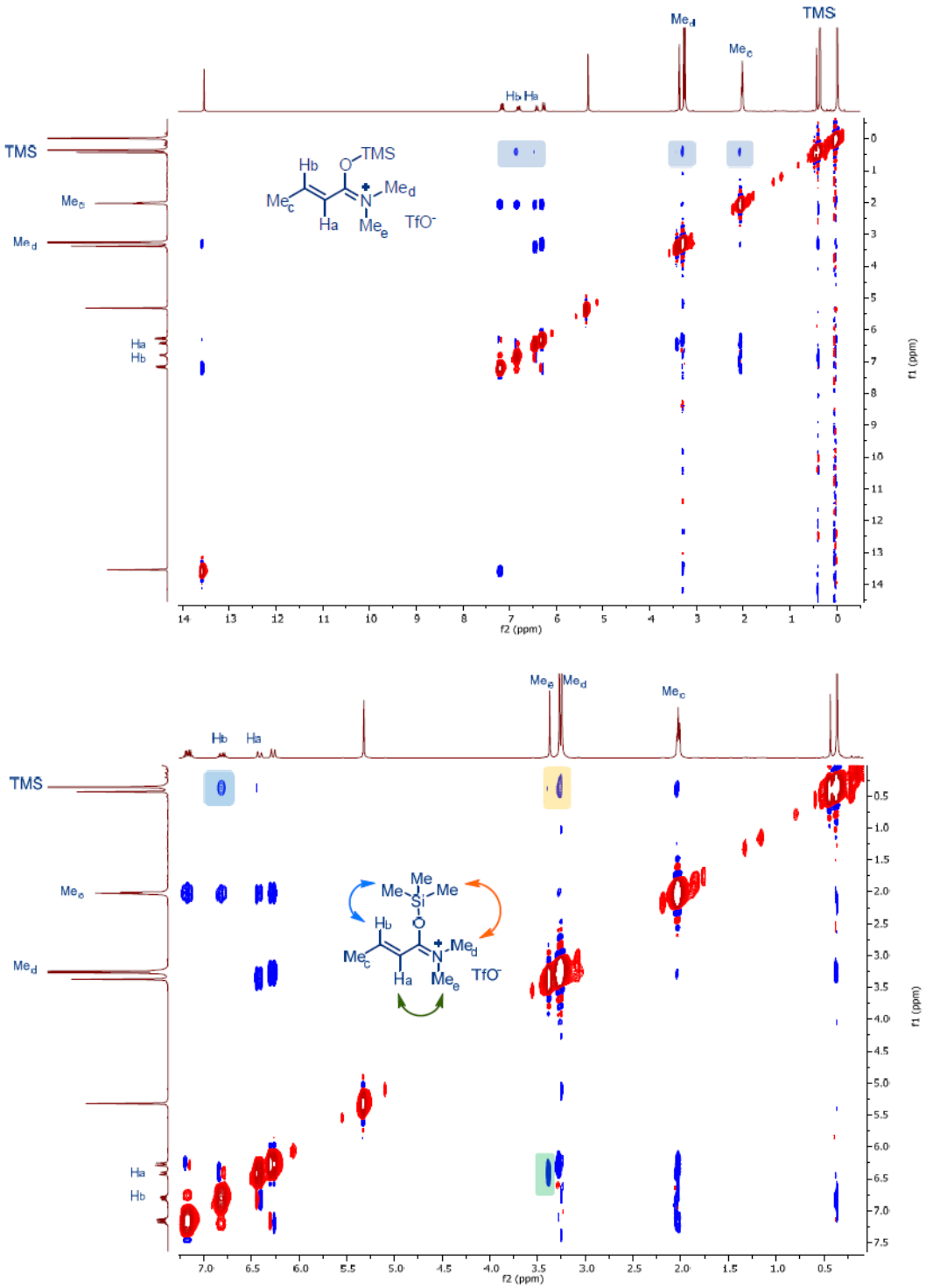


**Figure 9:** $^{1}$H-$^{1}$H-ROESY spectrum of the equimolar mixture of carboxamide **7** and TMSOTf and expansion. Cross-peaks between the TMS moiety and both Hb (blue) and one of the NMe groups (orange) and between the other NMe group and Ha (green) confirmed the O-silylation and the s-*trans* conformation.

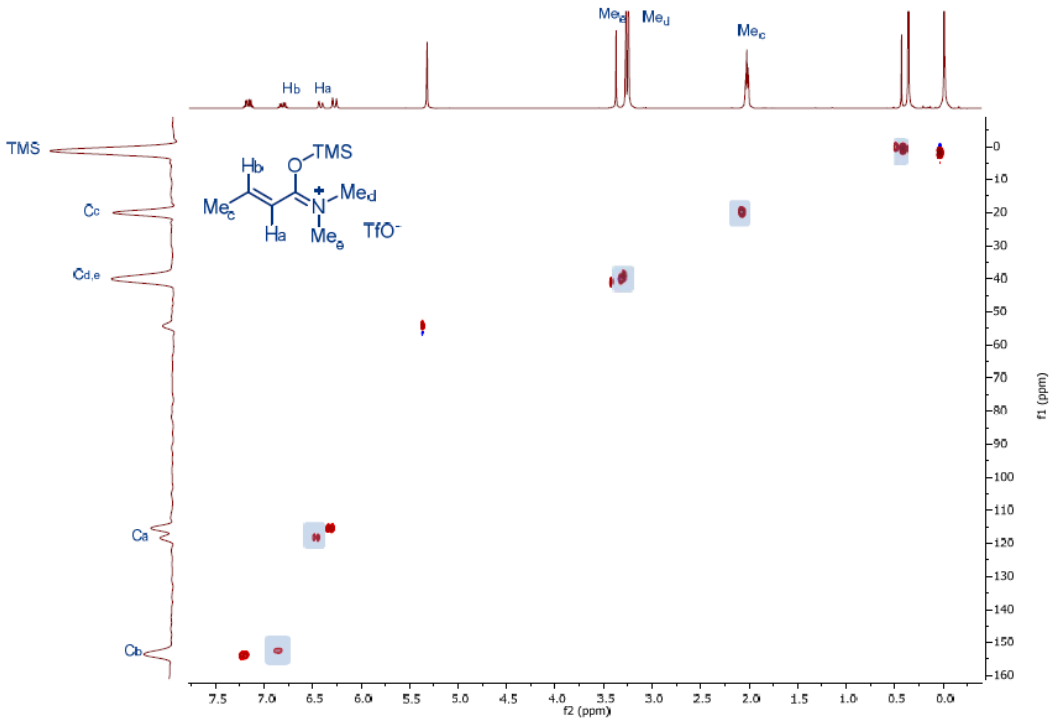


**Figure 10:** $^{1}H$-$^{13}C$-HSQCED spectrum of the equimolar mixture of carboxamide **7** and TMSOTf. TMS-carboxamide complex cross-peaks are highlighted.

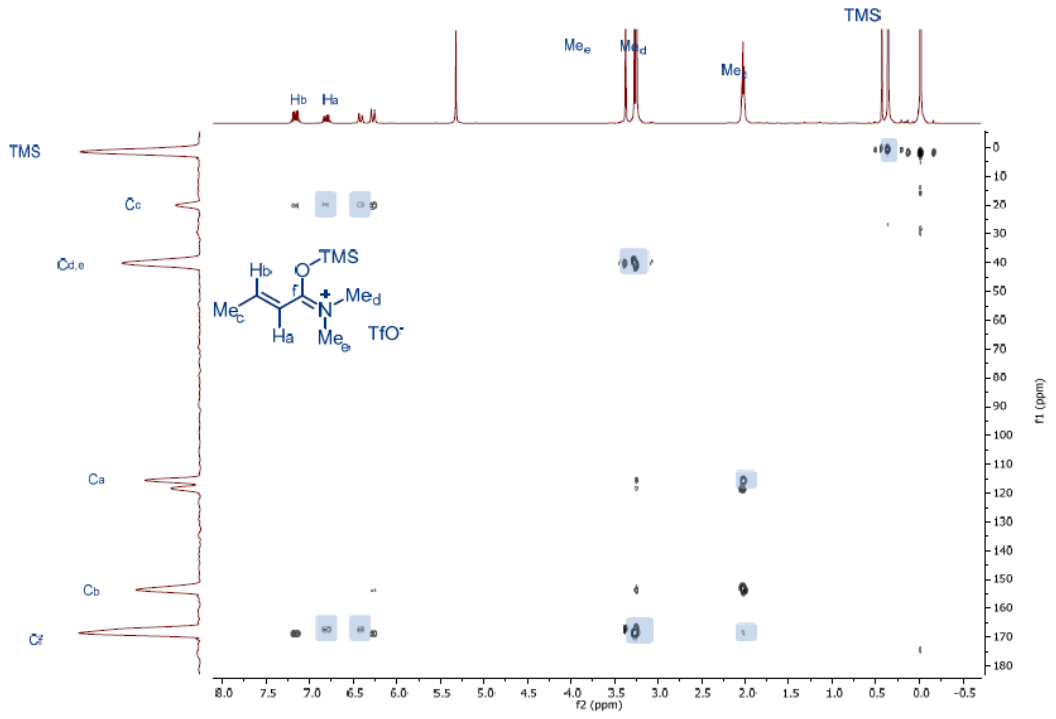


**Figure 11:** $^{1}H$-$^{13}C$-HMBC spectrum of the equimolar mixture of carboxamide **7** and TMSOTf. TMS-carboxamide complex cross-peaks are highlighted.

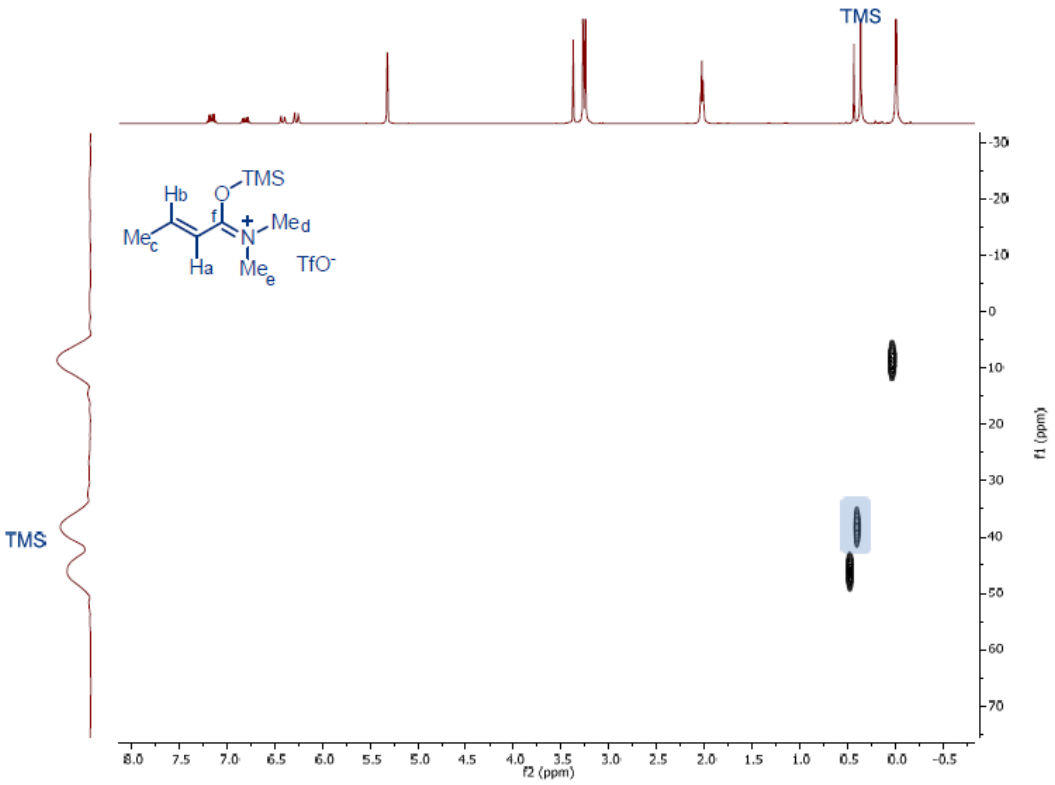


**Figure 12:** $^{1}H$-$^{29}Si$-HMBC spectrum of the equimolar mixture of carboxamide **7** and TMSOTf. TMS-carboxamide complex cross-peaks are highlighted.

According to our proposed catalytic cycle depicted in Scheme 6, the formation of transmetallated copper complex **6** is followed by the $\pi$-complexation with potentially activated carboxamide **8** or **9** to form species **10** or **10'**, followed by the formation of $\sigma$-complex intermediates **12** or **12'** (silyl enolate in case of TMSOTf and boron enolate in case of $BF_3{\cdot}Et_2O$). We initially anticipated the activated carboxamide to be LA-carboxamide complex **8**, the formation of which was indeed observed by $^{1}H$ NMR spectroscopy when adding either $BF_3{\cdot}Et_2O$ or TMSOTf to a solution of carboxamide in $CD_2Cl_2$. TMSOTf (16 $\mu$L, 0.088 mmol) was added to a solution of **7** (10 mg, 0.088 mmol) in $CD_2Cl_2$ (0.6 mL) in a dry NMR tube at −78 °C under $N_2$ atmosphere, leading to instantaneous formation of a new species, detected using NMR spectroscopy at −80 °C. Two carboxamide complexes were observed and characterized as TMS-carboxamide complex (assigned in Figure 8) and protonated carboxamide. Water derived from the carboxamide substrates partially hydrolizes TMSOTf resulting in the formation of TfOH, which can protonate the carboxamide as well. The formation of an iminium-type complex, placing the silyl moiety on the oxygen atom, was suggested by the deshielded $NMe_2$ groups in the new iminium moiety (up to 0.5 ppm downfield) and confirmed by a $^{1}H$-$^{1}H$ ROESY experiment (Figure 9). NMR spectroscopy also confirmed *s-trans* conformation. Full characterization was carried out by $^{1}H$-$^{13}C$-HSQCED (Figure 10), $^{1}H$-$^{13}C$-HMBC (Figure 11) and $^{1}H$-$^{29}Si$-HMBC (Figure 12).

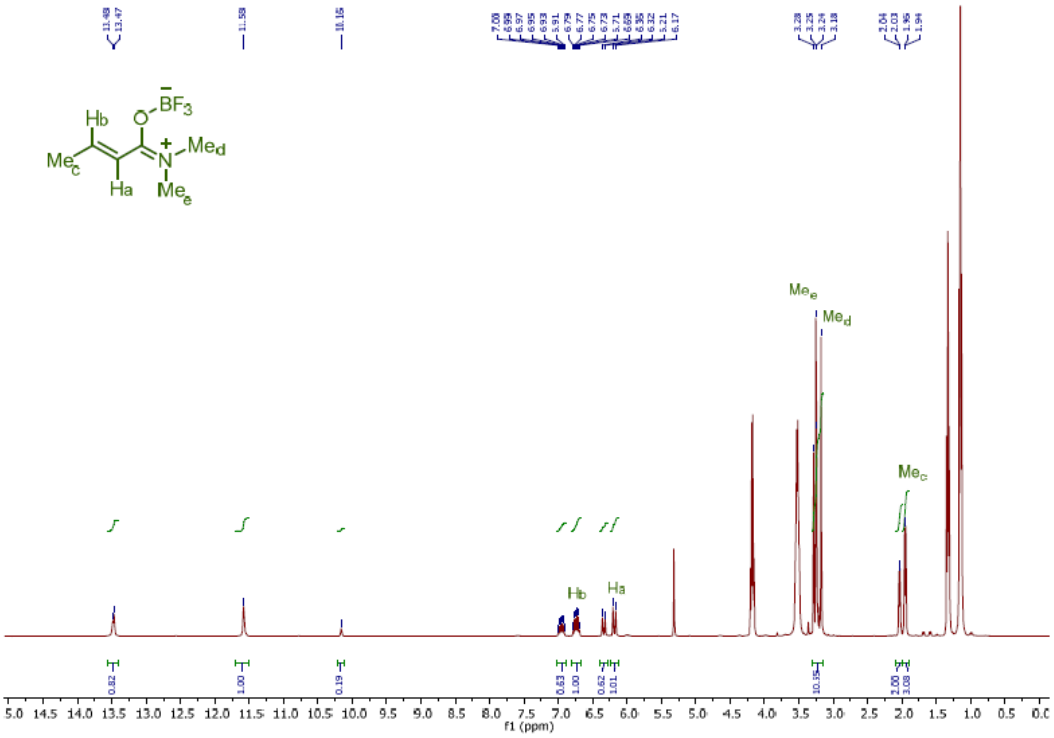


**Figure 13:** $^{1}$H NMR spectrum of the equimolar mixture of carboxamide **7** and $BF_3 \cdot Et_2O$.

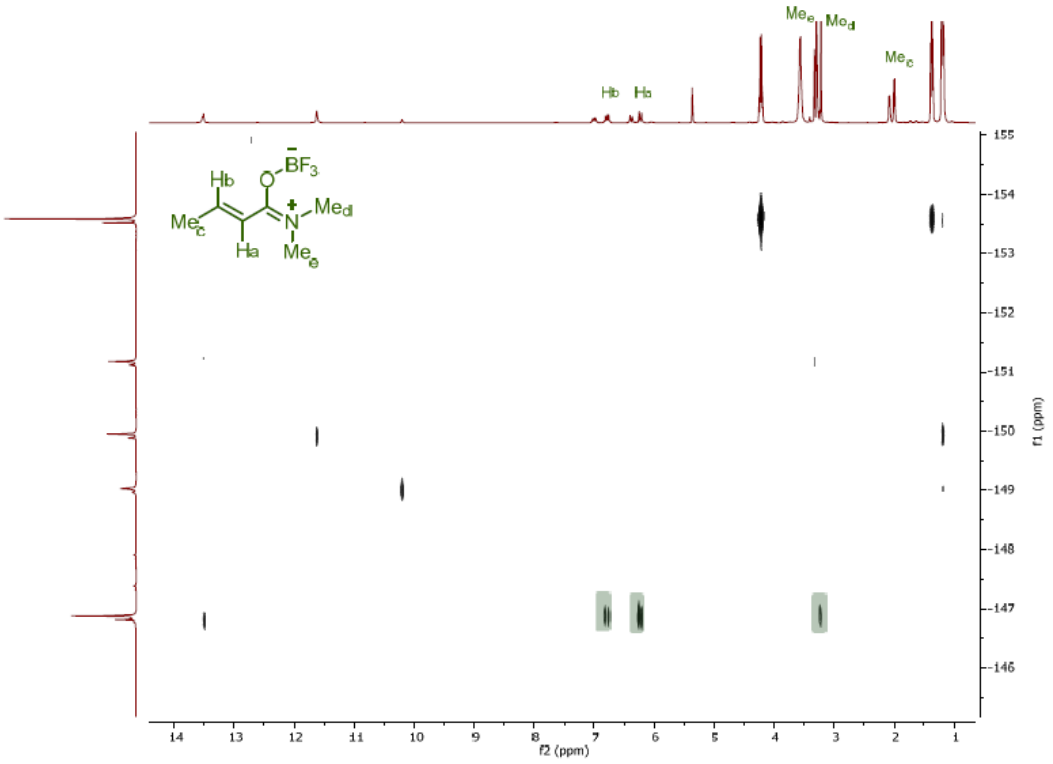


**Figure 14:** $^{1}$H-$^{19}$F-HOESY spectrum of the equimolar mixture of carboxamide **7** and $BF_3 \cdot Et_2O$. Cross-peak with the carboxamide moieties (green) and $^{19}$F signal at −147 ppm confirmed the formation of a complex. $BF_3$-carboxamide complex cross-peaks are highlighted.

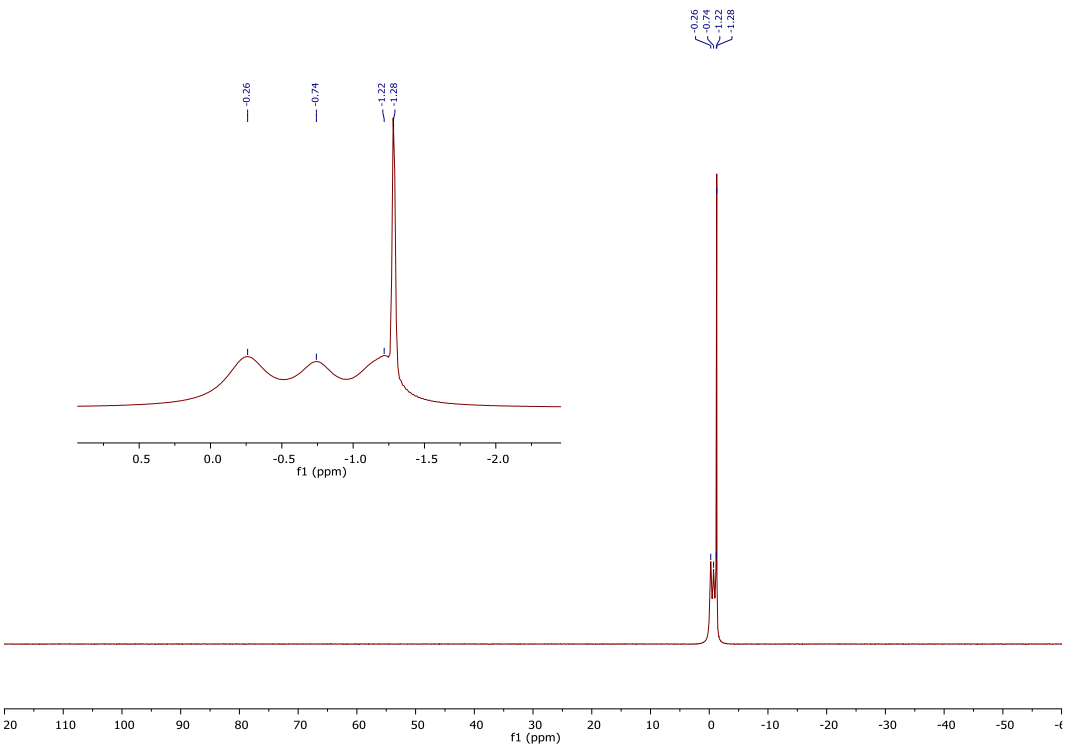


**Figure 15:** $^{11}$B-NMR spectrum of the equimolar mixture of carboxamide **7** and $BF_3{\cdot}Et_2O$.

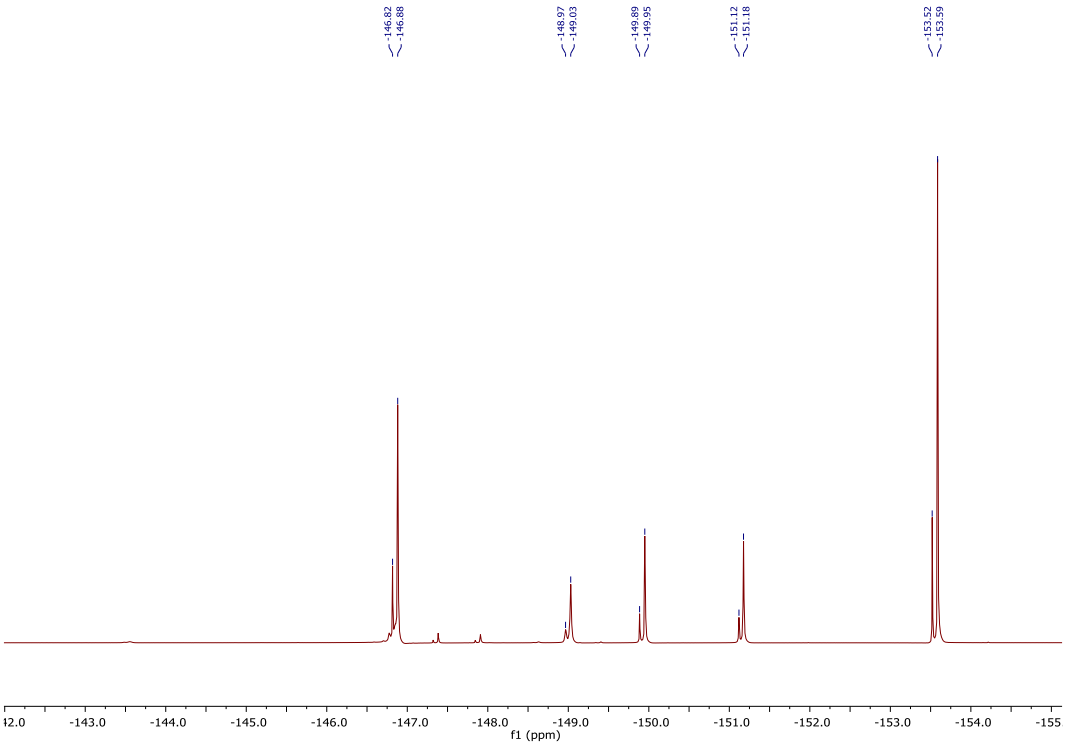


**Figure 16:** $^{19}$F-NMR spectrum of the equimolar mixture of carboxamide **7** and $BF_3{\cdot}Et_2O$.

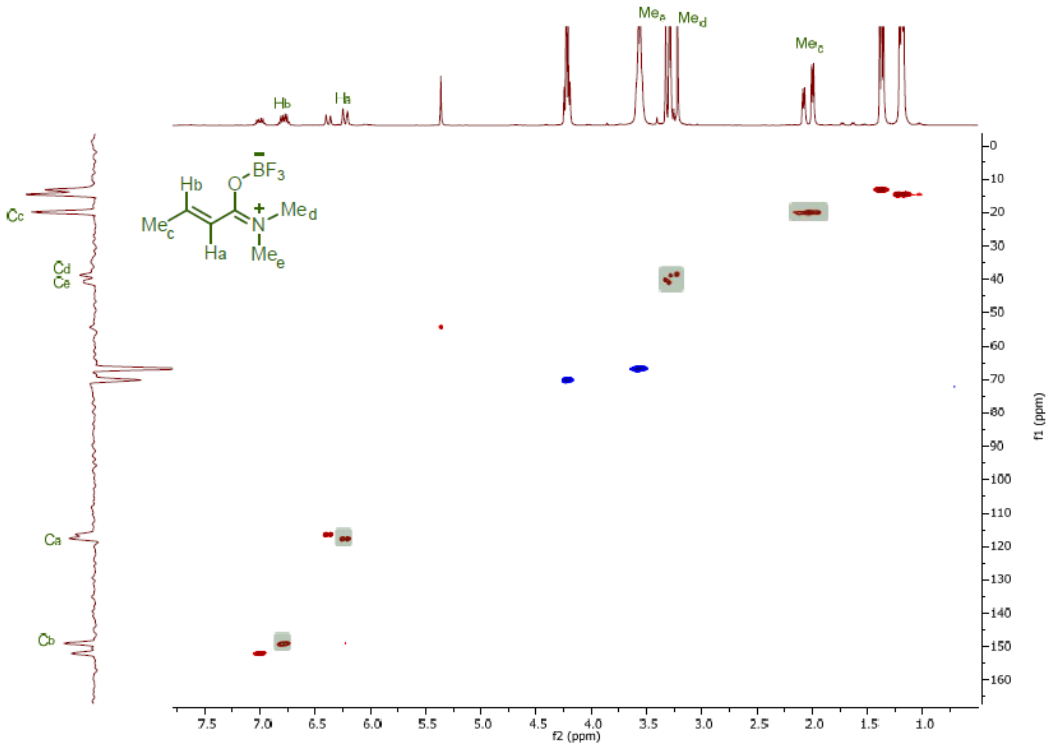


**Figure 17:** $^{1}$H-$^{13}$C-HSQCED spectrum of the equimolar mixture of carboxamide **7** and $BF_3$·$Et_2O$. $BF_3$-carboxamide complex cross-peaks are highlighted.

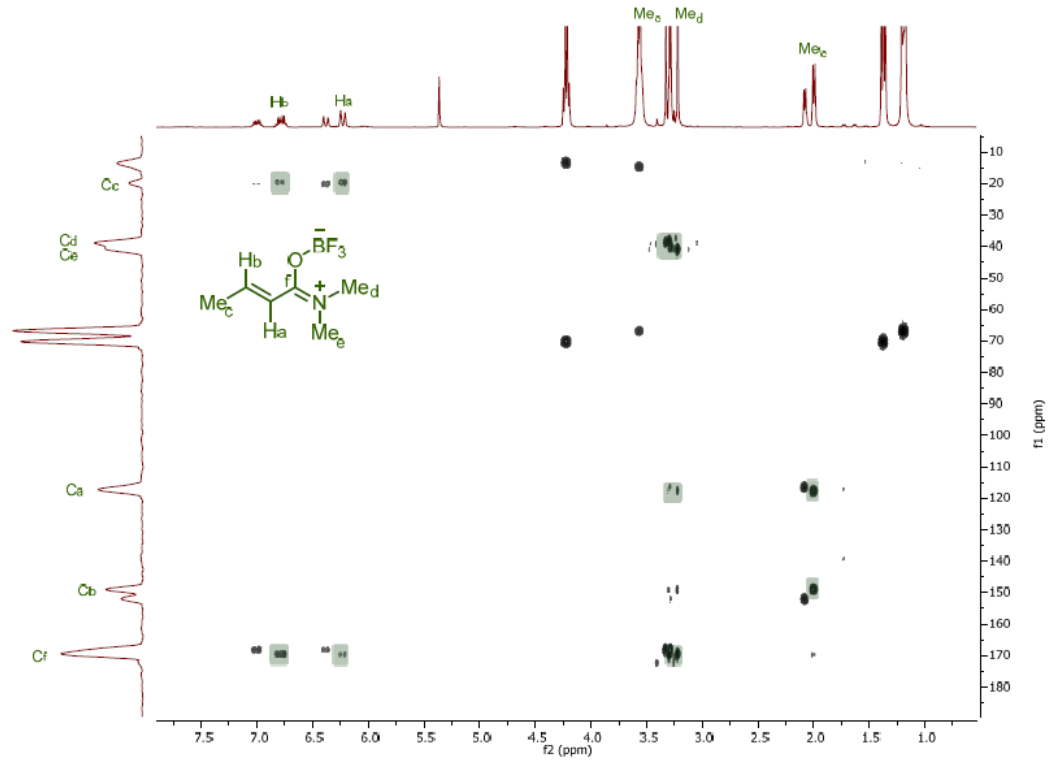


**Figure 18:** $^{1}$H-$^{13}$C-HMBC spectrum of the equimolar mixture of carboxamide **7** and $BF_3$·$Et_2O$. $BF_3$-carboxamide complex cross-peaks are highlighted.

Similarly, $BF_3$·$Et_2O$ (10 $\mu$L, 0.08 mmol) was added to a solution of carboxamide **7** (9 mg, 0.08 mmol) in $CD_2Cl_2$ (0.6 mL) in a dry NMR tube at −78 °C. Instantaneous formation of a new species at −80 °C was measured by NMR spectroscopy. In analogy with the experiment using TMSOTf two new carboxamide species were detected using $^{1}$H NMR (Figure 13). A

few other acidic proton peaks were detected as well due to the water present in the substrate. Formation of a carboxamide-$BF_3$ complex was confirmed by $^{1}H$-$^{19}F$-HOESY spectra (Figure 14) and fully characterized by $^{11}B$-NMR (Figure 15), $^{19}F$-NMR (Figure 16), $^{1}H$-$^{13}C$-HSQCED (Figure 17), and $^{1}H$-$^{13}C$-HMBC (Figure 18).

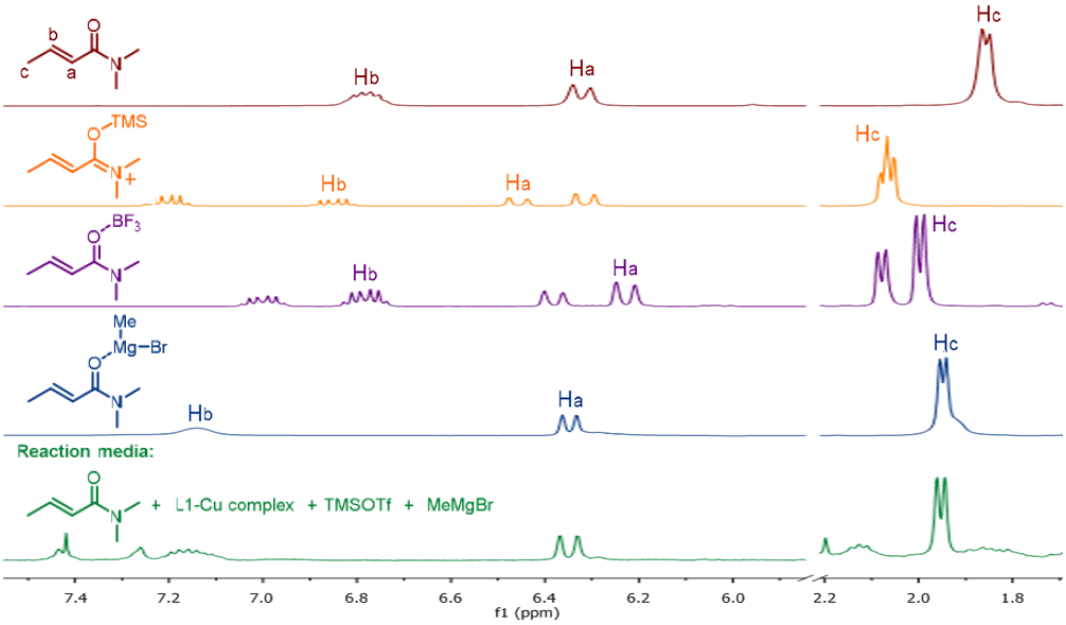


**Figure 19:** $^{1}H$ NMR spectra of LA-carboxamide complexes: free carboxamide (brown), with TMSOTf (orange), $BF_3{\cdot}Et_2O$ (purple), with MeMgBr (blue), the reaction media before completion (green).

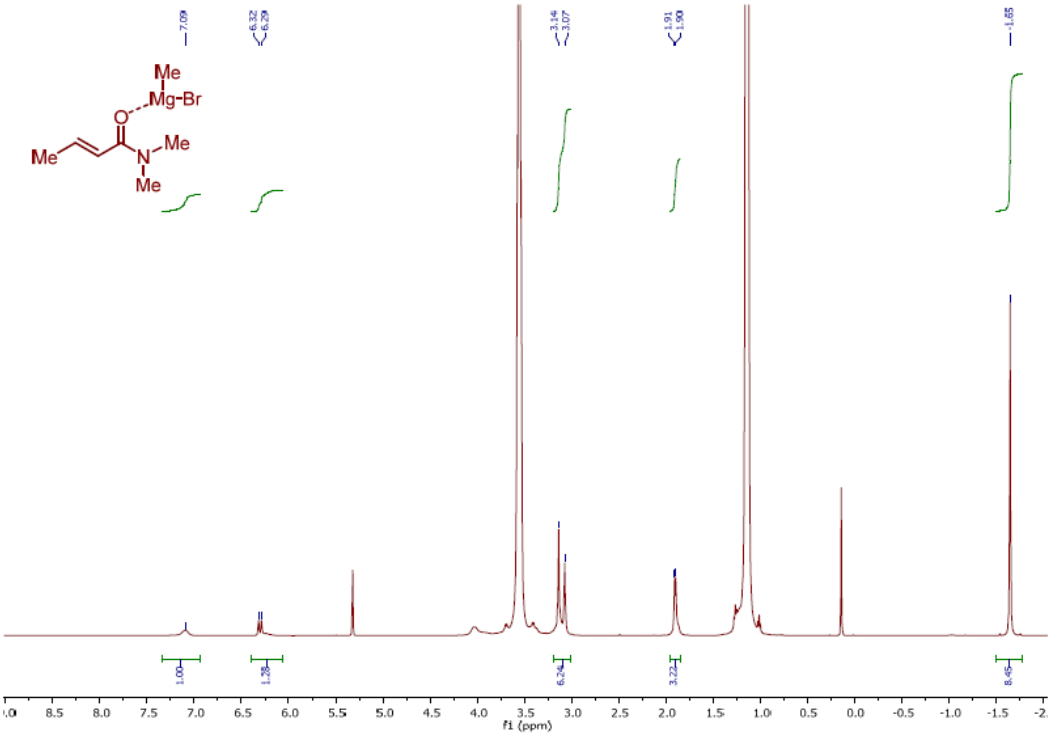


**Figure 20:** $^{1}H$ NMR spectrum of the mixture of carboxamide **1b** and MeMgBr.

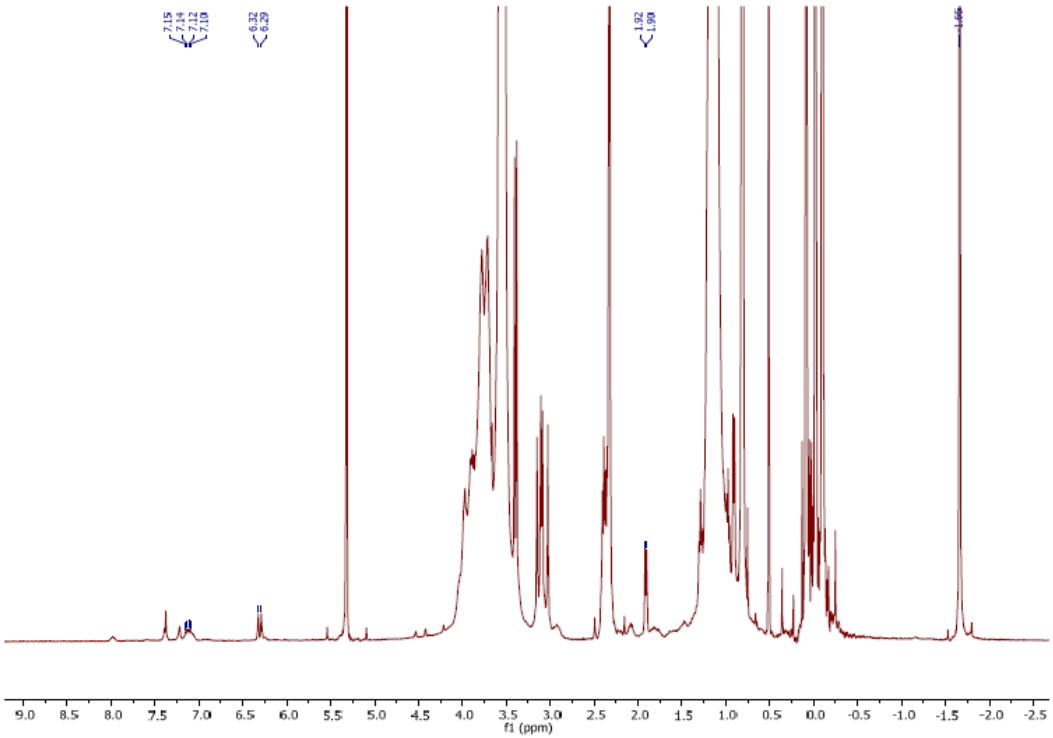


**Figure 21:** $^{1}$H NMR spectrum of the reaction media in the reaction of carboxamide **7** with MeMgBr in the presence of **L1**-CuBr complex and TMSOTf in $CD_2Cl_2$.

While these experiments with carboxamide **7** and LAs confirmed the formation of activated carboxamide species **8** (catalytic cycle in scheme 6), surprisingly, the subsequent addition of a stoichiometric amount of MeMgBr led to the formation of a new species corresponding to MeMgBr-carboxamide complex **9** (Figure 19). First we prepared complex **9** for comparison. A 3.0 M MeMgBr solution in $Et_2O$ (54 $\mu$L, 0.2 mmol) was added to a solution of amide **7** (6 mg, 0.05 mmol) in $CD_2Cl_2$ (0.6 mL) in a dry NMR tube at −78 °C. Instantaneous formation of a new species at −80 °C attributed to MeMgBr/carboxamide complex was measured by NMR spectroscopy (Figure 20). Only this species was observed in this experiment. Then a set of reactions was carried out in the presence of TMSOTf or $BF_3{\cdot}Et_2O$ in $CD_2Cl_2$ either directly in the NMR tubes or in dry Schlenk flasks at −78 °C and then measured at −80 °C (Figure 21, only the reaction media in the presence of TMSOTf are shown). In a flame-dried Schlenk tube equipped with septum and magnetic stirring bar, CuBr-($R$,$S_{Fe}$)-L1 complex (5.53 mg, 0.0075 mmol, 5 mol%) and amide **7** (17 mg, 0.15 mmol) were dissolved in $CD_2Cl_2$ (1.5 mL) and stirred under nitrogen atmosphere. After stirring at room temperature for 5 minutes, the reaction mixture was cooled to −60 °C and TMSOTf (52 $\mu$L, 0.30 mmol) was added. After 15 minutes, MeMgBr (100 $\mu$L, 0.30 mmol, 3.0 M in $Et_2O$) was added. Then the mixture was transferred to a NMR tube cooled to −78 °C and then measured by NMR spectroscopy at −80 °C. Regardless of the LA used, the only species observed in the reaction media corresponded to the complex **9** derived from the interaction between the carboxamide and MeMgBr (Figure 19). The same complex **9** was also detected when MeMgBr was added to the preformed TMSOTf-carboxamide or $BF_3{\cdot}Et_2O$ carboxamide complexes preformed in the absence of other reaction intermediates. These results suggest that MeMgBr replaces the Lewis acid and forms a more stable complex with the carboxamide.

On the one hand it seems reasonable to assume (catalytic cycle in Scheme 6) that $\pi$-complexation of species **6** with the relatively more stable activated carboxamide **9** would occur next, forming $\pi$-complex **10** in step 1. On the other hand, based on the Curtin–Hammett principle, direct formation of $\pi$-complex **10'** in step 2' cannot be excluded. Thus, the main question is at which stage the LA is involved in the catalytic cycle: before, during, or after oxidative addition step or during or after reductive elimination step. To answer this question further experiments were performed.

**Table 1: effect of different LAs in the Cu-catalyzed CA of EtMgBr to 13**[a]

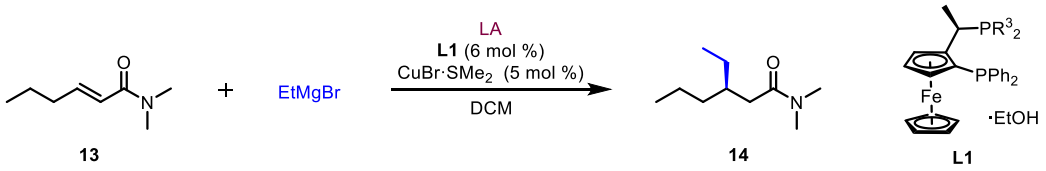


| Entry | LA | Yield [%][b] | *ee* [%][c] |
|---|---|---|---|
| 1 | TMSCl | <7 | nd |
| 2 | TMSBr | 44 | 78 |
| 3 | $BF_3{\cdot}Et_2O$ | 73 | 97 |
| 4 | TMSOTf | 92 | 92 |
| 5 | TBSOTf | 91 | 91 |
| 6 | TBDPSOTf | 84 | 88 |

[a]Reaction conditions: 0.1 M of **13** in DCM, $CuBr{\cdot}SMe_2$ (5 mol%), ligand **L1** (6 mol%), LA (2.0 equiv.), EtMgBr (2.0 equiv.), −78 °C, 18 h. [b]Yield of isolated **14**. [c]Enantiomeric excess was determined by HPLC on a chiral stationary phase.

Based on the *E*–*Z* isomerizations of $\alpha,\beta$-unsaturated carbonyl substrates often observed in copper-catalyzed CA reactions and specific isotope effects observed, the oxidative addition step is thought to be reversible, with the rate enhancement upon addition of TMSCl attributed to making the oxidative step irreversible.[19-25] To verify whether this holds true for the role of $BF_3{\cdot}Et_2O$ and TMSOTf in our reaction, more experiments were executed. A number of different LAs were tested varying in strength and sterics (Table 1). The results reveal clearly that the strength of the LA is crucial for our catalytic cycle, with the very weak TMSCl producing <7% conversion, the relatively stronger TMSBr a poor 44%, and the stronger TMS-, TBS- and TBDPS- substituted triflates as well as $BF_3{\cdot}Et_2O$ providing excellent results, both in terms of reactivity and selectivity. Furthermore, the nearly identical ees given by the three sterically varying triflates imply that the LA does not affect the enantiodiscrimination step. The differences observed in the *ee* using various LA are explained by different rates between the enantioselective Cu-catalyzed and the non-catalyzed racemic CA reactions.

Double-bond isomerization of the carboxamide substrate (**(*Z*)-13** to the more stable **(*E*)-13**) was studied as well (Table 2). Copper-catalyzed CA of MeMgBr or EtMgBr to **(*Z*)-13** led to the final products with absolute configuration opposite to that obtained with **(*E*)-13** when using $BF_3{\cdot}Et_2O$ and TMSOTf at −78 °C, respectively. No isomerization product to the more stable **(*E*)-13** was obtained using TMSOTf (Table 2, entries 3, 9, 11, 13, 16 and 20) or

with a little conversion up to 2.5% in the presence of $BF_3{\cdot}Et_2O$ (Table 2, entries 2, 8, 10, 12, 14 and 18). This is consistent with the interpretation that step 2 (or 3') of the catalytic cycle is not reversible.

**Table 2: Cu-catalyzed CA of MeMgBr or EtMgBr to (*E*)- or (*Z*)-13[a]**

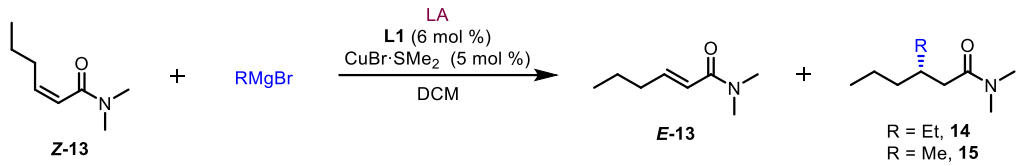


| Entry | **13** | **L1**/Cu [mol%] | LA | RMgBr | **(*Z*):(*E*):14**[b] **(*Z*):(*E*):15**[b] | *ee* [%][c] | Conf. of **14** or **15** |
|---|---|---|---|---|---|---|---|
| 1 | ***Z*** | 5 | – | – | 100:0:– | – | – |
| 2 | ***Z*** | – | $BF_3{\cdot}Et_2O$ | – | 100:0:– | – | – |
| 3 | ***Z*** | – | TMSOTf | – | 100:0:– | – | – |
| 4 | ***Z*** | – | – | MeMgBr | 100:0:0 | – | – |
| 5 | ***Z*** | – | – | EtMgBr | 100:0:0 | – | – |
| 6 | ***Z*** | 5 | – | MeMgBr | 100:0:0 | – | – |
| 7 | ***Z*** | 5 | – | EtMgBr | 100:0:0 | – | – |
| 8 | ***Z*** | – | $BF_3{\cdot}Et_2O$ | MeMgBr | 100:0:0 | – | – |
| 9 | ***Z*** | – | TMSOTf | MeMgBr | 100:0:0 | – | – |
| 10 | ***Z*** | – | $BF_3{\cdot}Et_2O$ | EtMgBr | 100:0:0 | – | – |
| 11 | ***Z*** | – | TMSOTf | EtMgBr | 98:0:2 | – | – |
| 12 | ***Z*** | 5 | $BF_3{\cdot}Et_2O$ | – | 95.5:2.5:– | – | – |
| 13 | ***Z*** | 5 | TMSOTf | – | 100:0:– | – | – |
| 14 | ***Z*** | 5 | $BF_3{\cdot}Et_2O$ | MeMgBr | 75.8:1.6:22.6 | 99 | (*S*)-15 |
| 15 | ***E***[d] | 5 | $BF_3{\cdot}Et_2O$ | MeMgBr | –:35:65 | 99 | (*R*)-15 |
| 16 | ***Z*** | 5 | TMSOTf | MeMgBr | 93:0:7 | 46 | (*S*)-15 |
| 17 | ***E***[d] | 5 | TMSOTf | MeMgBr | –:8:92 | 99 | (*R*)-15 |
| 18 | ***Z*** | 5 | $BF_3{\cdot}Et_2O$ | EtMgBr | 37.4:1.6:61 | 96 | (*S*)-14 |
| 19 | ***E***[d] | 5 | $BF_3{\cdot}Et_2O$ | EtMgBr | –:6:94 | 97 | (*R*)-14 |
| 20 | ***Z*** | 5 | TMSOTf | EtMgBr | 70:0:30 | 33 | (*S*)-14 |
| 21 | ***E***[d] | 5 | TMSOTf | EtMgBr | –:6:94 | 92 | (*R*)-14 |

[a]Reaction conditions: 0.16 mmol of **(*Z*)-13** in 1.6 mL of DCM, $CuBr{\cdot}SMe_2$ (5 mol%), ligand **L1** (6 mol%), LA (2.0 equiv.), RMgBr (2.0 equiv.), −78 °C, 18 h. [b]The ratio between **(*Z*)-13**:**(*E*)-13**:**14** or **(*Z*)-13**:**(*E*)-13**:**15** was determined by $^1$H-NMR. [c]Enantiomeric excess was determined by HPLC on a chiral stationary phase. [d]0.2 mmol of **(*E*)-13** were used in this case.

Combining the results on the strength of the LA, its lack of effect on the enantiodiscrimination, the lack of isomerization and Cu-catalyzed ACA in the absence of LA, and all the discussed experimental data, we believe that the LA is almost certainly involved in one of the steps preceding reductive elimination (step 4), making the oxidative addition overall irreversible (catalytic cycle , Scheme 6). Strong LA is either required to increase the $\pi$-acidity of the $\pi$-complex (as in $\pi$-complex **10'** formed in step 2') or to trap the magnesium enolate $\sigma$-complex **11** into the more stable silyl or boron enolate $\sigma$-complex **11'** (step 3). In both scenarios, that cannot be distinguished with the current data, the resulting more stable silyl or boron enolate $\sigma$-complex **11'** is expected to undergo faster reductive elimination than the magnesium enolate $\sigma$-complex **11**. Further support for the formation

of $\sigma$-complex **11'** comes from the fact that only Mg activated carboxamide **9** and silyl or boron enolates of the CA addition products (Figure 22) are observed, with no traces of **8** or Mg-enolate of the CA-product throughout the reaction. For the experiments confirming the structure of the CA-enolate products see the following discussion.

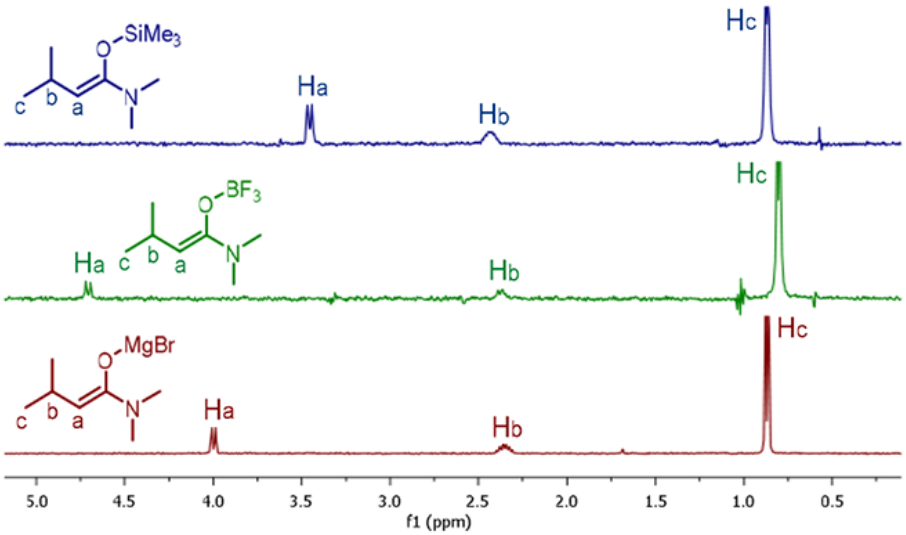


**Figure 22:** Types of enolates formed as end product of the CA of MeMgBr to carboxamide in the reaction using TMSOTf (blue), $BF_3{\cdot}Et_2O$ (green), and in the absence of LA (brown) determined by TOCSYs experiments.

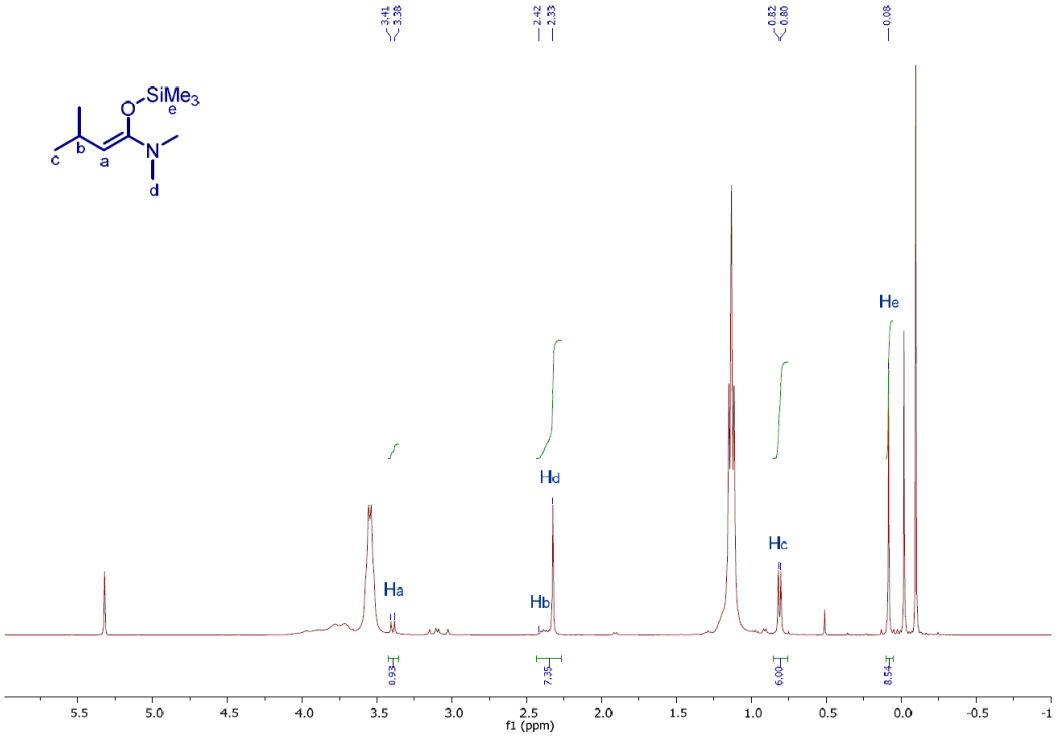


**Figure 23:** $^1$H NMR spectrum of the crude of the reaction in the presence of TMSOTf.

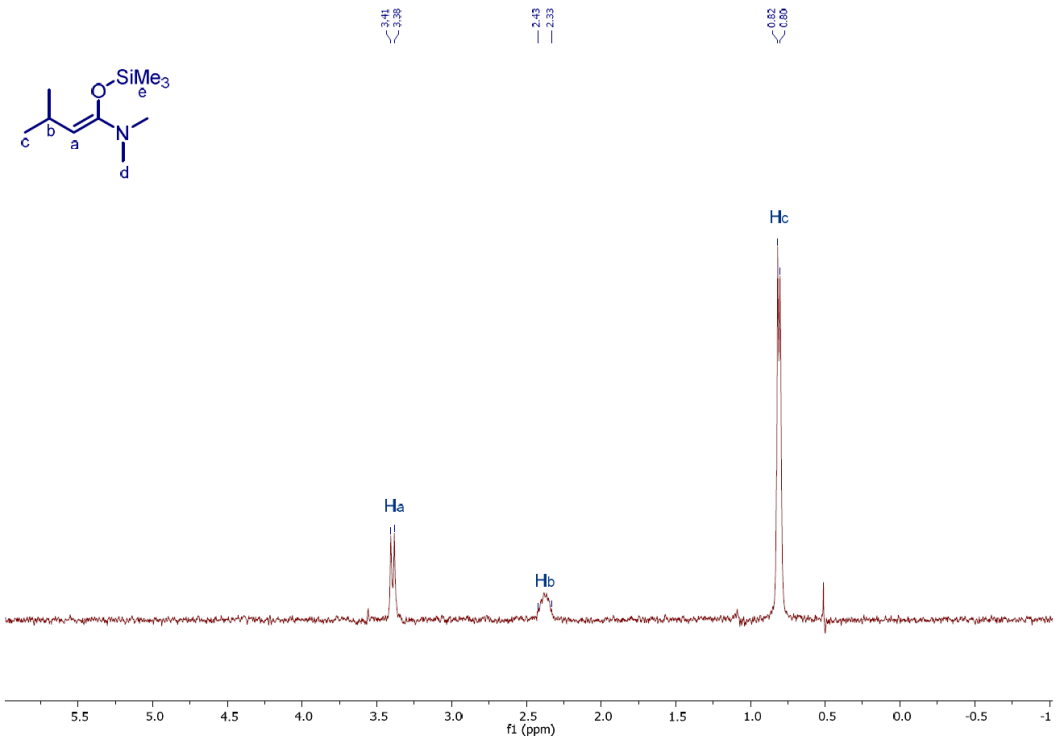


**Figure 24:** TOCSY experiment (irradiating nucleus Ha) of the crude of the reaction in the presence of TMSOTf.

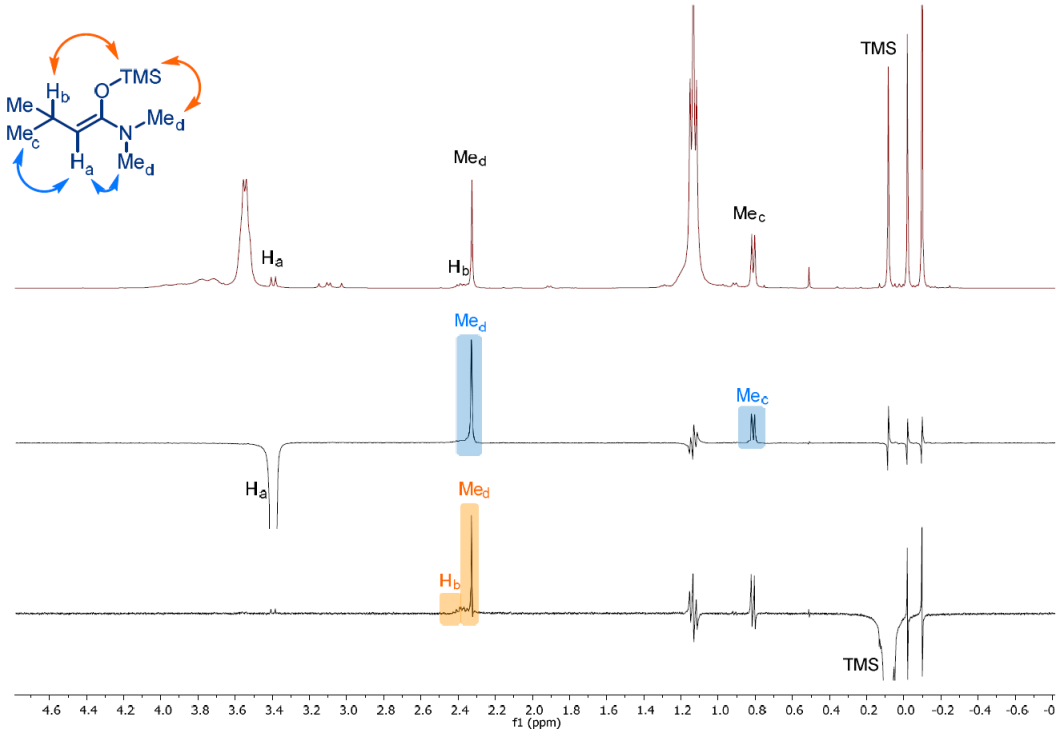


**Figure 25:** 1D ROESY experiments of the crude of the reaction in the presence of TMSOTf. *Z*-enolate configuration was determined by observation of NOE between the TMS moiety and Hb (orange) and between Ha and NMe moiety and gem-dimethyl moiety (Mec, blue).

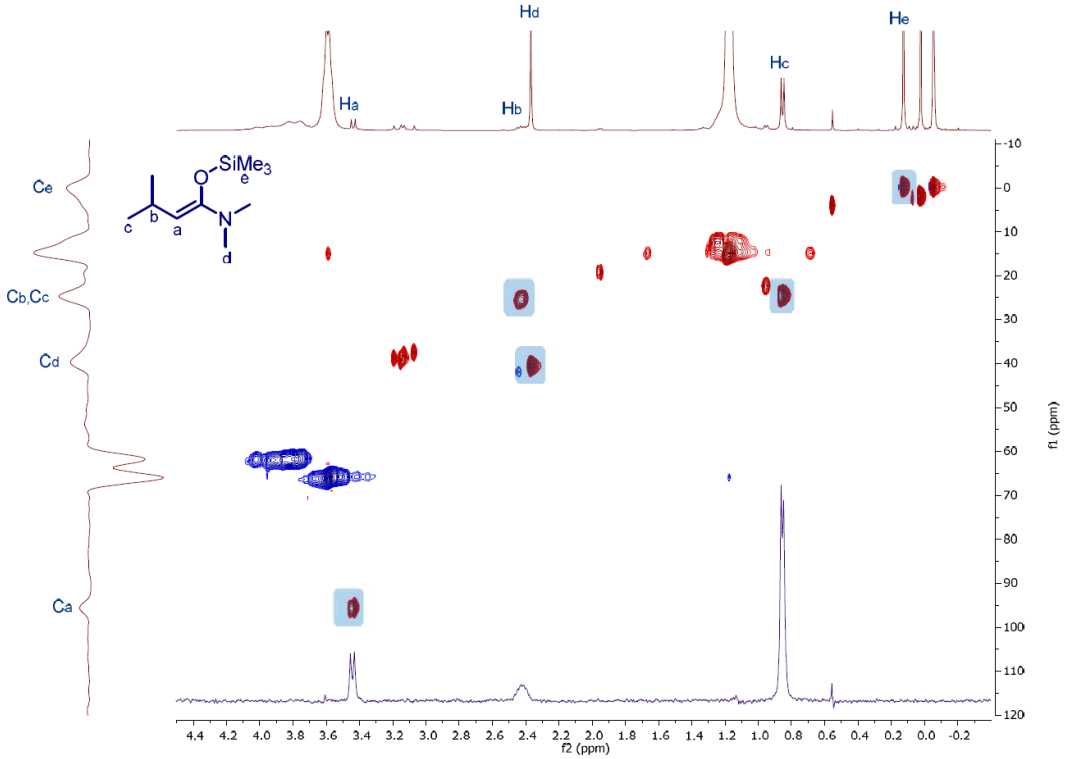


**Figure 26:** $^{1}H$-$^{13}C$-HSQCED spectrum of the crude of the reaction in the presence of TMSOTf. TMS-enolate peaks are highlighted.

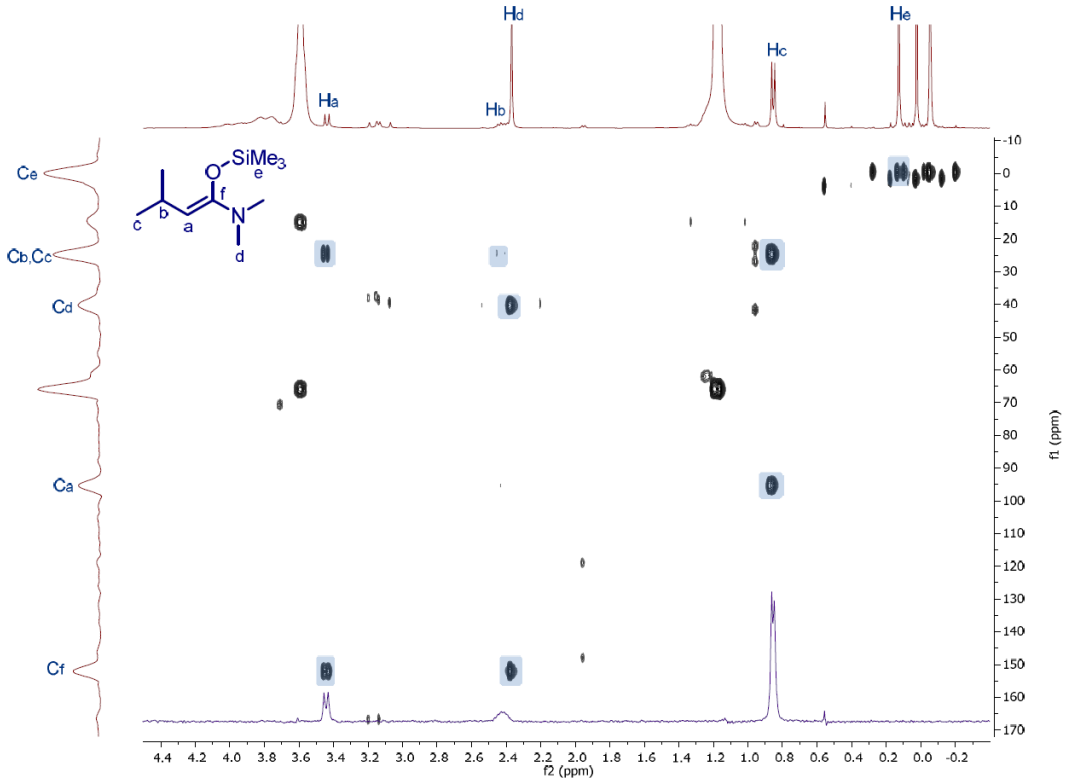


**Figure 27:** $^{1}H$-$^{13}C$-HMBC spectrum of the crude of the reaction in the presence of TMSOTf. TMS-enolate peaks are highlighted.

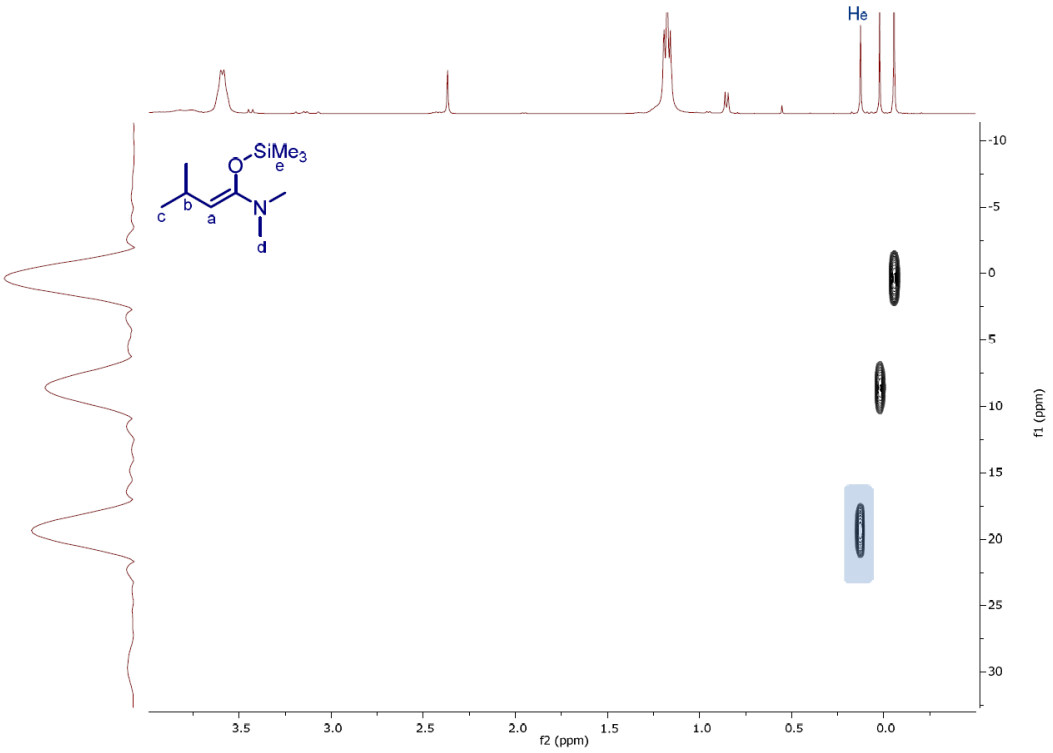


**Figure 28:** $^{1}$H-$^{29}$Si-HMBC spectrum of the crude of the reaction in the presence of TMSOTf. TMS-enolate peaks are highlighted.

The structure of the final product of the reaction, namely the enolates, was determined by analysis of the reaction crude before quench in $CD_2Cl_2$. First we performed the catalytic ACA in the presence of TMSOTf, aiming at the formation of the silyl enolate. In a flame-dried Schlenk tube equipped with septum and magnetic stirring bar, CuBr-(*R*,$S_{Fe}$)-**L1** complex (5.53 mg, 0.0075 mmol, 5 mol%) and amide **7** (17 mg, 0.15 mmol) were dissolved in $CD_2Cl_2$ (1.5 mL) and stirred under nitrogen atmosphere. After stirring at room temperature for 5 min., the reaction mixture was cooled to −60 °C and TMSOTf (52 $\mu$L, 0.30 mmol) was added. After 15 min., MeMgBr (100 $\mu$L, 0.30 mmol, 3.0 M in $Et_2O$) was added. After stirring at −60 °C for 18 h, the mixture was transferred to a NMR tube followed by measurement at −80 °C. The final product in the reaction mixture was identified as a TMS-enolate (Figure 23), based on a TOCSY experiment (Figure 24). (*Z*)-configuration was assigned to the enolate, based on series of 1D ROESY experiments (Figure 25). Full characterization by $^{1}$H-$^{13}$CHSQCED (Figure 26), $^{1}$H-$^{13}$C-HMBC (Figure 27) and $^{1}$H-$^{29}$Si-HMBC (figure 28) was carried out.

Then we performed the catalytic ACA in the presence of $BF_3{\cdot}Et_2O$ to form the boron enolate. In a flame-dried Schlenk tube equipped with septum and magnetic stirring bar, CuBr-(*R*,$S_{Fe}$)-**L1** complex (5.53 mg, 0.0075 mmol, 5 mol%) and amide **7** (17 mg, 0.15 mmol) were dissolved in $CD_2Cl_2$ (1.5 mL) and stirred under nitrogen atmosphere. After stirring at room temperature for 5 min., the reaction mixture was cooled to −60 °C and $BF_3{\cdot}Et_2O$ (37 $\mu$L, 0.30 mmol) was added. After 15 min., MeMgBr (100 $\mu$L, 0.30 mmol, 3.0 M in $Et_2O$) was added. After stirring at −60 °C for 18 h, the mixture was transferred to a NMR tube, cooled and measured by NMR spectroscopy at −80 °C. A $BF_3$-enolate structure was assigned based on $^{1}$H NMR (Figure 29). Enolate proton (Ha) was detected in the crude and with a TOCSY

experiment (Figure 30) Ha, Hb, Hc protons were assigned. Full characterization of the enolate was done by $^{1}H$-$^{13}C$-HSQCED (Figure 31) and $^{1}H$-$^{13}C$-HMBC (Figure 32) experiments.

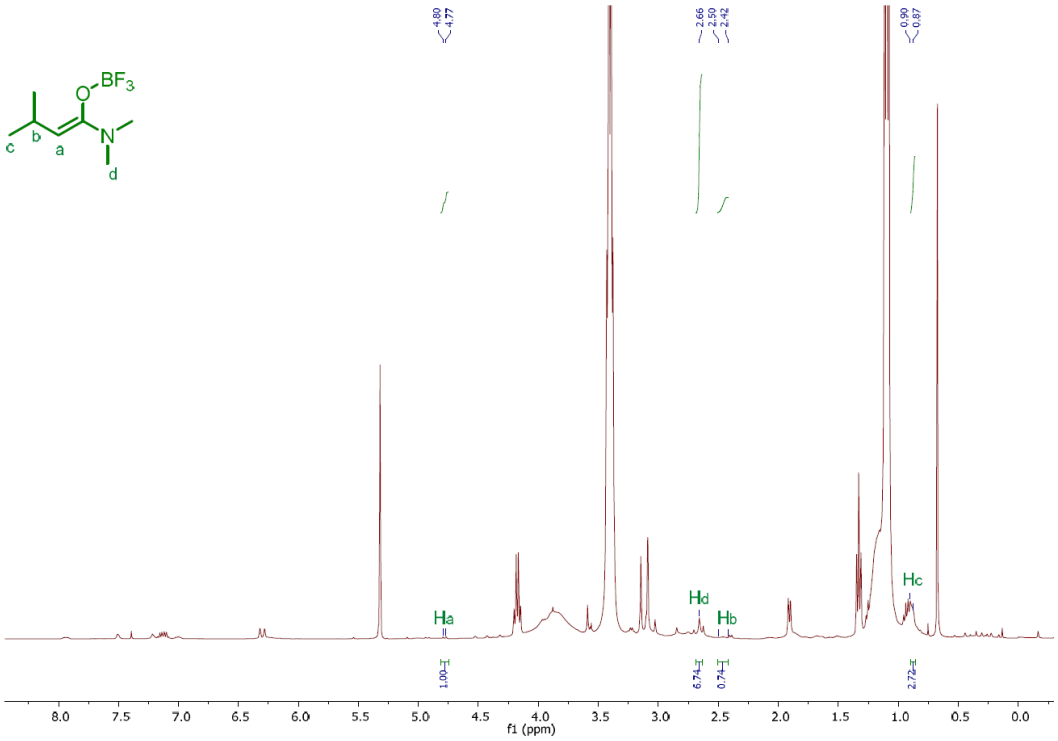


**Figure 29:** $^{1}H$ NMR spectrum of the crude of the reaction in the presence of $BF_3{\cdot}Et_2O$.

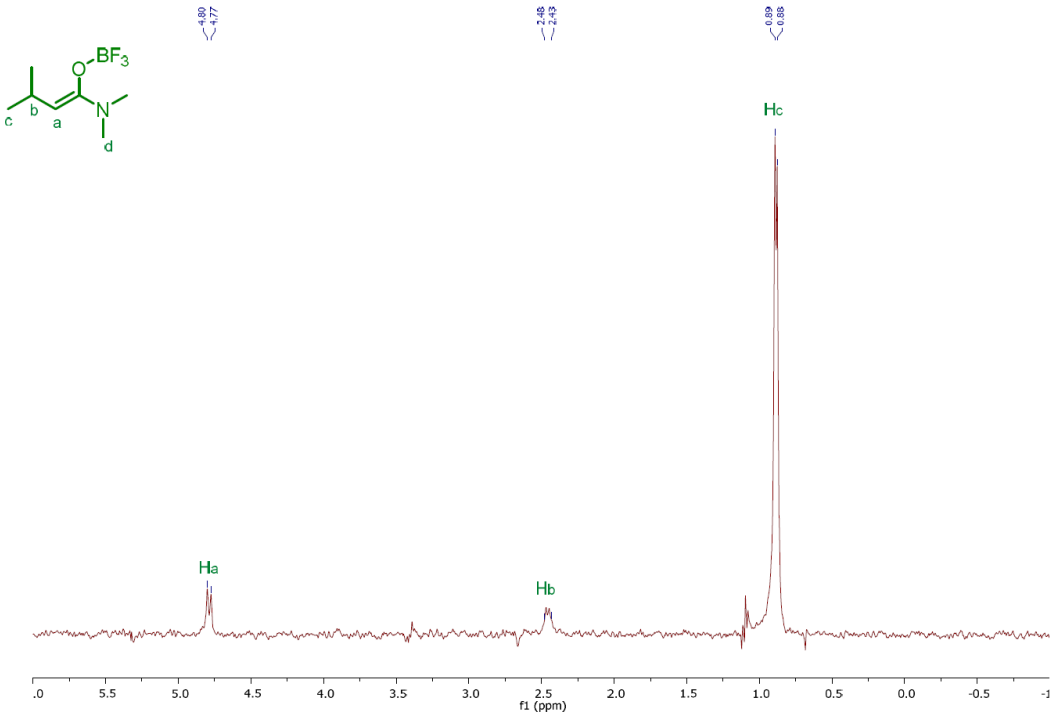


**Figure 30:** TOCSY experiment (irradiating nucleus Ha) of the crude of the reaction in the presence of $BF_3{\cdot}Et_2O$.

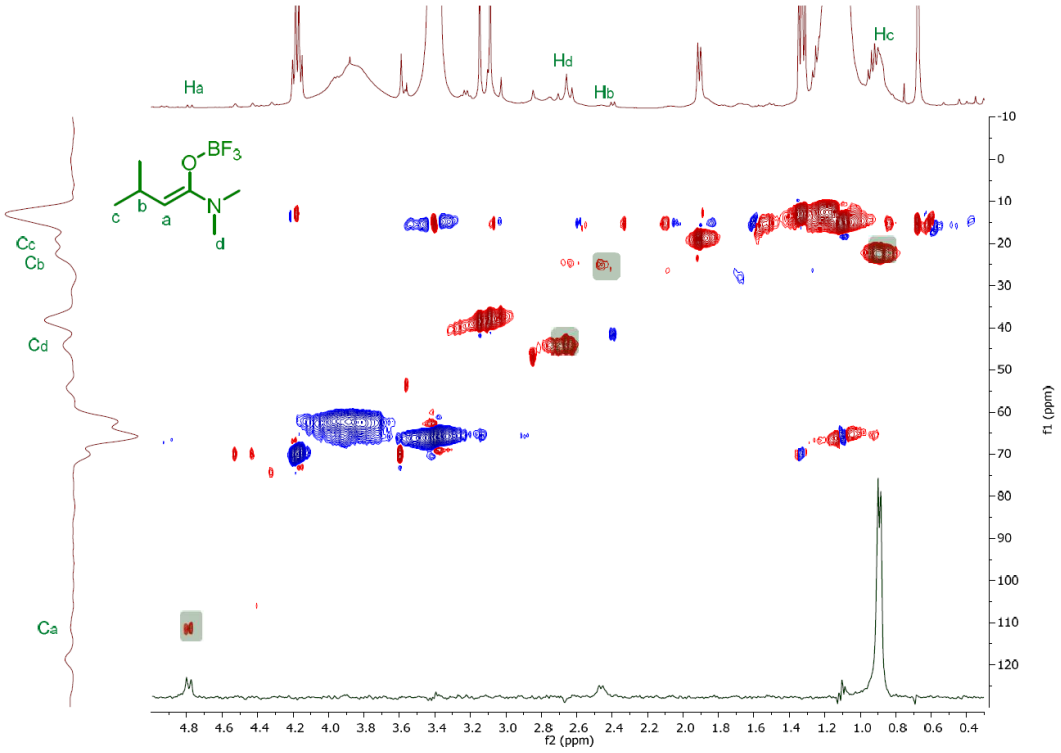


**Figure 31:** $^{1}H$-$^{13}C$-HSQCED spectrum of the crude of the reaction in the presence of $BF_3{\cdot}Et_2O$. $BF_3$-enolate peaks are highlighted.

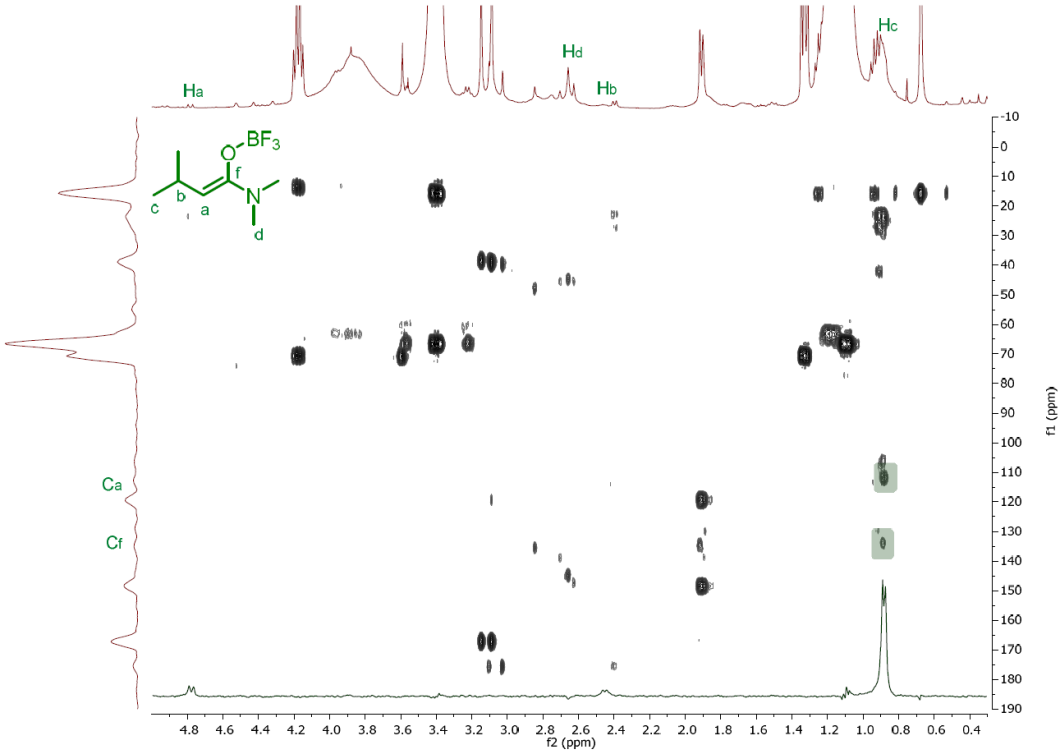


**Figure 32:** $^{1}H$-$^{13}C$-HMBC spectrum of the crude of the reaction in the presence of $BF_3{\cdot}Et_2O$. $BF_3$-enolate peaks are highlighted.

However, the configuration of the enolate could not be determined by HOESY experiments since no clear cross-peak $^{1}H$-$^{19}F$ was observed. To prove that the enolate we observed in this case is not a magnesium enolate we prepared Mg-enolate independently for comparison in the absence of LA and fully characterized it by NMR spectroscopy. A 3.0 M

MeMgBr solution in $Et_2O$ (67 $\mu$L, 0.2 mmol) was added to a solution of amide 1a (12 mg, 0.10 mmol) in $CD_2Cl_2$ (0.6 mL) in a dry NMR tube under $N_2$ atmosphere. After 18 h the mixture was measured by NMR spectroscopy at −80 °C. A Mg-enolate structure was assigned based on $^1$H NMR (Figure 33). Enolate proton (Ha) was detected in the crude and a TOCSY experiment (Figure 34) was carried out to assign the spin system (Ha, Hb, Hc). Full characterization by $^1$H-$^{13}$C-HSQCED (Figure 35) and $^1$H-$^{13}$CHMBC (Figure 36) was carried out.

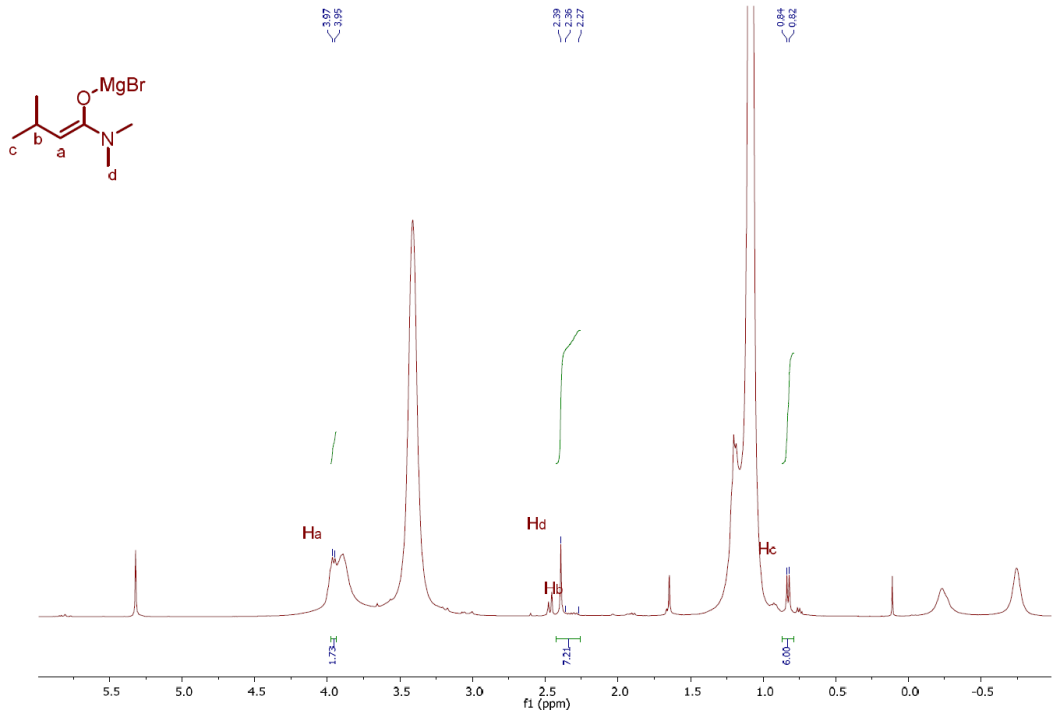


**Figure 33:** $^1$H NMR spectrum of the crude of the reaction in the absence of Lewis acid.

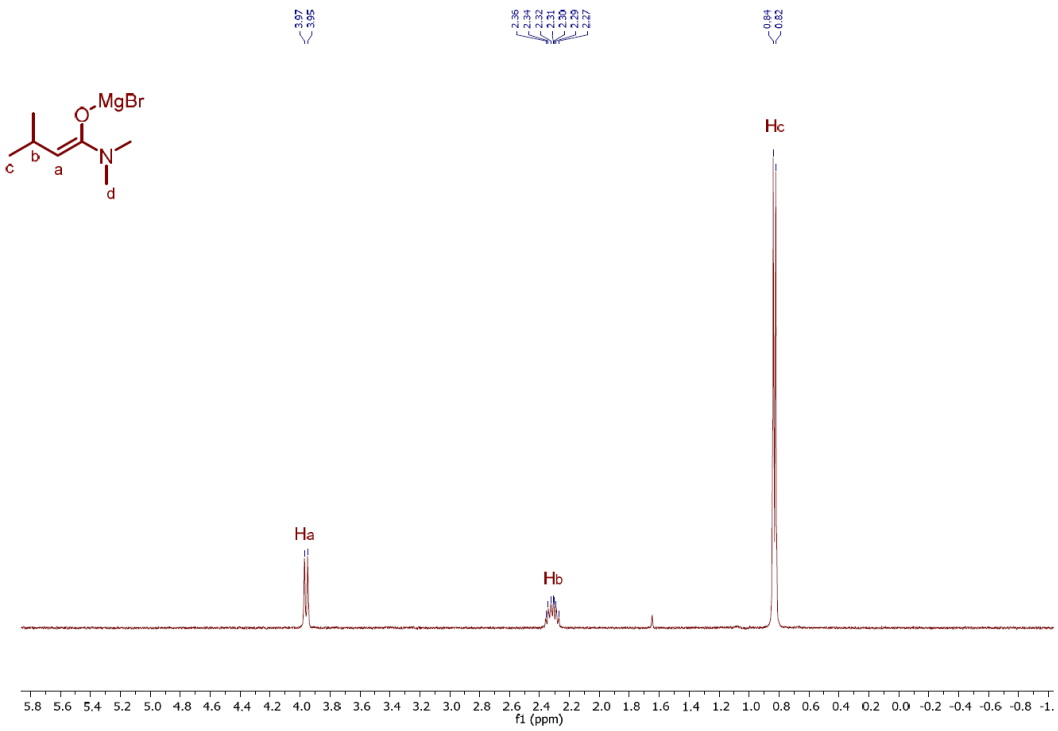

**Figure 34:** TOCSY experiment (irradiating nucleus Ha) of the crude of the reaction in the absence of Lewis acid.

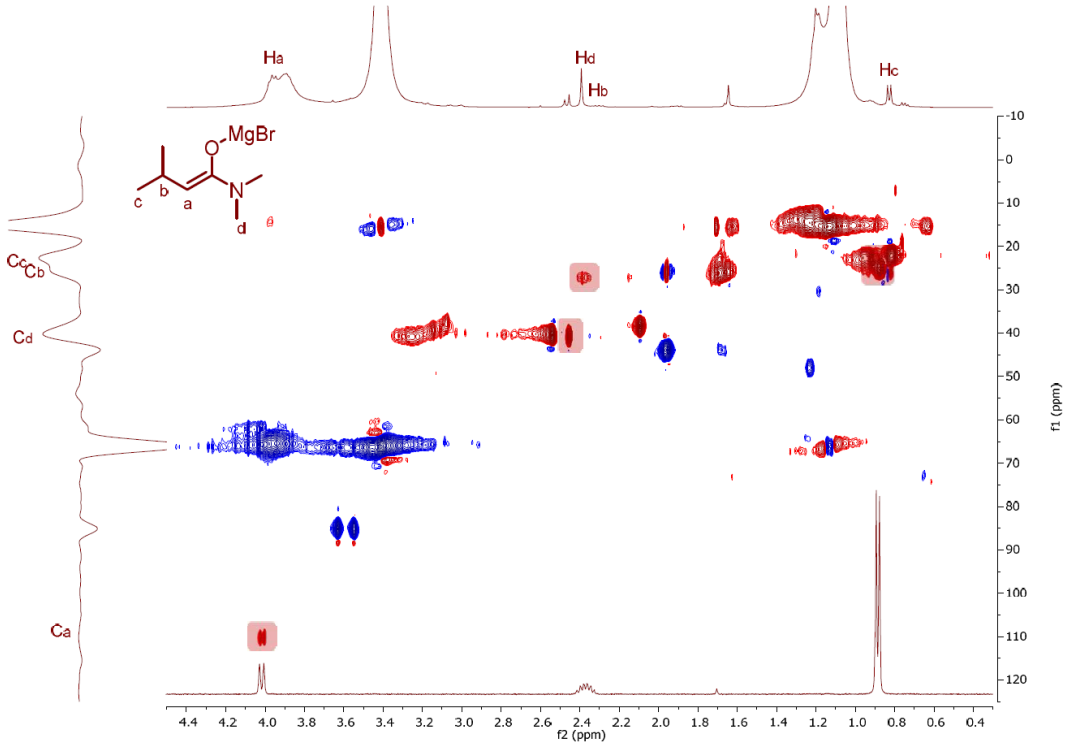


**Figure 35:** $^{1}H$-$^{13}C$-HSQCED spectrum of the crude of the reaction in the absence of Lewis acid. Mg-enolate peaks are highlighted.

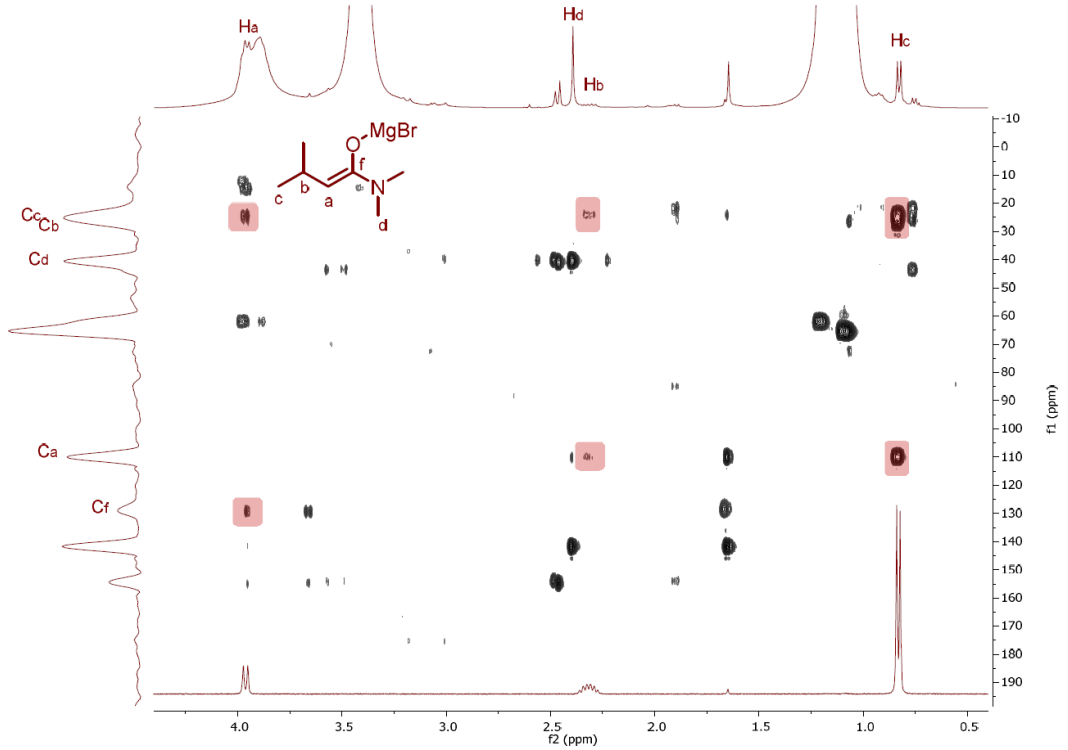


**Figure 36:** $^{1}H$-$^{13}C$-HMBC spectrum of the crude of the reaction in the absence of Lewis acid. Mg-enolate peaks are highlighted.

This set of experiments shows that three different enolates, namely TMS-enolate (in the presence of TMSOTf), $BF_3$-enolate (in the presence of $BF_3{\cdot}Et_2O$) and Mg-enolate (in the absence of Lewis acid) are formed in the reaction mixture, depending on the reaction components (Figures 22–36).

## 3.3 Conclusions

Our mechanistic studies identified the structure of various species involved in the LA-enabled, Cu-catalyzed ACA of Grignards to *α*,*β*-unsaturated carboxamides and support the notion that the role of the LA is in the enhancement of the copper-catalyzed pathway. As a result, LA allows both the ACA to occur as well as to outcompete the blank reactions that occur at higher temperatures. Furthermore, the experimental data point to a very similar mechanistic behavior for both LAs employed in this ACA of Grignard reagents to *α*,*β*-unsaturated carboxamides, namely $BF_3{\cdot}Et_2O$ and TMSOTf. The unexpected compatibility observed in our catalytic system between highly reactive Grignard reagents, LAs, and phosphine ligands was found to be due to the remarkable stability of the active catalyst toward the deleterious effect of LAs.

## 3.4 Experimental section

### 3.4.1 General experimental information

All reactions using oxygen- and/or moisture-sensitive materials were carried out with anhydrous solvents (*vide infra*) under a nitrogen atmosphere using oven-dried glassware and standard Schlenk techniques. Flash column chromatography was performed using Merck 60 Å 230–400 mesh silica gel. Thin layer chromatography was performed using 0.25 mm E. Merck silica plates (60F-254). Unless otherwise indicated, the products were visualized by UV and $KMnO_4$ staining. NMR data was collected on Varian VXR400 ($^1H$ at 400.0 MHz; $^{13}C$ at 100.58 MHz) equipped with a 5 mm *z*-gradient broadband probe. Chemical shifts are reported in parts per million (ppm) relative to residual solvent peak ($CDCl_3$, $^1H$: 7.26 ppm; $^{13}C$: 77.16 ppm; $CD_2Cl_2$, $^1H$: 5.32 ppm; $^{13}C$: 53.84 ppm). Coupling constants are reported in Hertz. Multiplicity is reported with the usual abbreviations (s: singlet, d: doublet, t: triplet, q: quartet, m: multiplet). Variable-temperature NMR spectra were acquired on a Bruker Avance III spectrometer paired with an Ascend 400 MHz magnet and BBFO dual-resonance probe. All temperatures were calibrated prior to acquisition with an external pure MeOH reference. $^1H$ TOCSY and ROESY experiments were carried out with 9.6 kHz and 4.54 kHz spinlocking fields, and the ROESY mix time was set to 400 ms. $^1H$-$^{19}F$ HOESY experiments utilized a mix time of 350 ms. $^1H$-$^{13}C$ HSQCED spectra were recorded with the $^1J_{CH}$ constant set to 145 Hz while the $^1H$-$^{13}C$ and $^1H$-$^{29}Si$ HMBC spectra were recorded with a $^nJ_{XH}$ constant set to 8 Hz and 10 Hz, respectively. 1D $^{19}F$ spectra were acquired with inverse-gated $^1H$ decoupling. 1D $^{31}P$ spectra were acquired with $^1H$ decoupling during the relaxation delay and acquisition time and thus are non-quantitative. Exact mass spectra were recorded on a LTQ Orbitrap XL apparatus with ESI ionization. Enantiomeric excess were determined by chiral HPLC analysis using a Shimadzu LC-10ADVP HPLC equipped with a Shimadzu SPD-M10AVP diode array detector.

### 3.4.2 Chemicals

Unless otherwise indicated, reagents and substrates were purchased from commercial sources and used as received. Dry solvents were freshly collected from a dry solvent purification system prior to use. Inert atmosphere experiments were performed with standard Schlenk techniques with dried $P_2O_5$ nitrogen gas. Grignard reagents were purchased from Sigma-Aldrich: EtMgBr, MeMgBr (2.0 M in $Et_2O$). All Grignard reagents were titrated by $^1H$ NMR before use. Unless otherwise noted *α,β*-unsaturated carboxamides substrates were prepared following the literature methods (*vide infra*). Chiral ligand **L1** were purchased from Sigma Aldrich and Solvias. All reported compounds were characterized by $^1H$ NMR and compared with literature data. All new compounds were fully characterized by $^1H$ and $^{13}C$ NMR and HRMS techniques.

### 3.4.3 Determination of absolute configuration

The absolute configuration of **14** and **15** was assigned by analogy to **2a** and **3h** in chapter 2.

### 3.4.4 Procedures and characterization of products

**(*E*)-*N*,*N*-Dimethylbut-2-carboxamide (7)[29]**

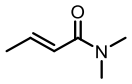

7

A solution of acyl chloride (0.96 mL, 10 mmol) in 6.3 mL dry $Et_2O$ was cooled to 0 °C in an ice-bath. Anhydrous dimethylamine (2.0 M in THF, 10 mL, 20 mmol) was added for over 5 min and the reaction mixture was allowed to warm to room temperature (12 h). The solvents were evaporated under reduced pressure. Product **7** was obtained as a colorless liquid after column chromatography ($SiO_2$, $Et_2O$) in 90 % yield. $^1H$ NMR ($CDCl_3$, 400 MHz): $\delta$ 6.87 (dq, $J$ = 15.0, 6.9 Hz, 1H, C*H*=CH), 6.27 (dq, $J$ = 15.0, 1.7 Hz, 1H, CH=C*H*), 3.06 (s, 3H, NC$H_3$), 2.99 (s, 3H, NC$H_3$), 1.87 (dd, $J$ = 6.9, 1.7 Hz, 3H, C$H_3$CH).

**(*E*)-*N*,*N*-Dimethylhex-2-enamide ((*E*)-13)[29]**

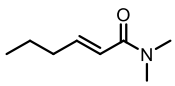

(*E*)-13

To a cold 0 °C solution of (*E*)-hex-2-enoic acid (570.7 mg, 5 mmol) in DCM (4 mL) was added thionyl chloride (438 $\mu$L, 6 mmol) and dry DMF (14 $\mu$L). The solution was then stirred at room temperature for 2 h and concentrated under reduced pressure to remove residual thionyl chloride. The resulting residue was redissolved in DCM (4 mL), cooled at 0 °C and dimethylamine (2.0 M in THF, 4 mL, 8 mmol) was added. Dry triethylamine (6.6 mmol) was added and stirring was continued at ambient temperature (3 h). The solvent was removed under reduced pressure and DCM (14 mL) was added. The organic phase was washed with dilute hydrochloric acid (2.0 M, 2 mL × 2), water (3 mL × 2), and brine (4 mL), and dried over $MgSO_4$. After removal of the solvent, product **(*E*)-13** was obtained as a

colorless oil in 86% yield. $^1$H NMR ($CDCl_3$, 400 MHz): $\delta$ 6.86 (dt, $J$ = 15.1, 7.0 Hz, 1H, C*H*=CH), 6.24 (dt, $J$ = 15.1, 1.3 Hz, 1H, CH=C*H*), 3.07 (s, 3H, NC$H_3$), 2.99 (s, 3H, NC$H_3$), 2.23-2.14 (m, 2H, C$H_2$CH), 1.54-1.43 (m, 2H, C$H_2$CH$_3$), 0.93 (t, $J$ = 7.4 Hz, 3H, CH$_2$C$H_3$).

**(*Z*)-*N*,*N*-Dimethylhex-2-enamide ((*Z*)-13)**

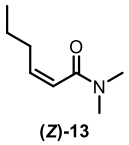

(*Z*)-13

To a solution of *N*,*N*-dimethylacetamide (465 $\mu$L, 5 mmol) in dry THF (15 mL) cooled to −78 °C, a 1.0 M solution of LDA in THF (4.5 mmol, 4.5 mL) was slowly added and the mixture was stirred for 30 minutes at −78 °C. Then, TMSCl (571 $\mu$L, 4.5 mmol) was added and the mixture was stirred for 1 h at 0 °C and, afterwards, cooled down again to −78 °C. A 1.0 M solution of LDA in THF (4.5 mmol, 4.5 mL) was slowly added and the reaction mixture was stirred for 30 minutes at −78 °C. Finally, butyraldehyde (405 $\mu$L, 4.5 mmol) was added and the mixture was stirred overnight at −78 °C. The reaction was quenched by addition of MeOH (1.0 mL) and 1.0 M HCl aqueous solution (10 mL), stirred at room temperature for 45 minutes and extracted with $Et_2O$ (15 mL × 3). The combined organic layers were dried over $MgSO_4$ and concentrated under reduced pressure. The crude product was purified by column chromatography on silica gel ($SiO_2$, pentane:$Et_2O$ = 1:1) to afford product **(*Z*)-13** as a colorless oil [39% yield]. $^1$H NMR ($CDCl_3$, 400 MHz): $\delta$ 5.95 (dt, $J$ = 11.7, 1.3 Hz, 1H, C*H*=CH), 5.89 (dt, $J$ = 11.7, 7.3 Hz, 1H, CH=C*H*), 3.00 (s, 6H, N(C$H_3$)$_2$), 2.35-2.27 (m, 2H, C$H_2$CH=CH), 1.49-1.39 (m, 2H, CH$_2$C$H_2$CH$_3$), 0.92 (t, $J$ = 7.3 Hz, 3H,CH$_2$C$H_3$). $^{13}$C NMR ($CDCl_3$, 100 MHz): $\delta$ 168.0, 141.0, 122.0, 37.6, 35.1, 31.3, 22.3, 13.8.

**(*R*)-*N*,*N*-Dimethyl-3-ethyl-hexanamide ((*R*)-14)**

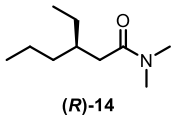

(*R*)-14

In a flame-dried Schlenk tube equipped with septum and magnetic stirring bar, CuBr·SMe$_2$ (2.06 mg, 0.01 mmol, 5 mol%) and ligand ($R$,$S_{Fe}$)-**L1** (7.68 mg, 0.012 mmol, 6 mol%) were dissolved in 2.0 mL DCM and stirred under nitrogen atmosphere for 20 min. The substrate **(*E*)-13** (0.2 mmol) was added at once. After stirring for 5 min. at RT the reaction mixture was cooled down to −78 °C, followed by addition of $BF_3$·$Et_2O$ (50 $\mu$L, 0.4 mmol) or TMSOTf (72 $\mu$L, 0.4 mmol). After 20 min., EtMgBr was added by hand in about 1 min. After stirring for 18 h, the reaction was quenched with MeOH followed by addition of saturated aqueous $NH_4Cl$ solution and warming up to RT. The reaction mixture was extracted with DCM (10 mL × 3). Combined organic phases were dried over $MgSO_4$, filtered and solvents were evaporated on a rotary evaporator. Product **(*R*)-14** was obtained as a colorless oil after column chromatography ($SiO_2$, pentane:$Et_2O$ = 1:1). $^1$H NMR ($CDCl_3$, 400 MHz): $\delta$ 3.00 (s, 3H, NC$H_3$), 2.93 (s, 3H, NC$H_3$), 2.21 (dd, $J$ = 15.1, 7.1 Hz, 1H, C*H*HCO), 2.20 (dd, $J$ = 15.1, 6.7 Hz, 1H, CH*H*CO), 1.91-1.81 (m, 1H, C*H*CH$_2$), 1.36-1.21 (m, 5H, C$H_2$CH$_3$, CH$_2$C$H_2$CH$_3$), 1.24-1.18 (m, 1H, CH*H*CH$_3$), 0.87 (d, $J$ = 7.0 Hz, 3H, C$H_3$CH), 0.85 (t, $J$ = 7.5 Hz, 3H, C$H_3$CH$_2$). $^{13}$C

NMR ($CDCl_3$, 100 MHz): $\delta$ 173.1, 37.8, 37.6, 36.1, 35.9, 35.5, 26.4, 19.9, 14.5, 11.0. HRMS (ESI+, m/Z): calcd. for $C_{10}H_{22}NO$ $[M+H]^+$: 172.1696, found: 172.1696. HPLC: Chiracel-OBH, *n*-heptane/*i*-PrOH 95:5, 0.5 mL/min, 40 °C, detection at 210 nm. Retention time (min): 10.4 (minor) and 11.5 (major).

**(*S*)-*N*,*N*-Dimethyl-3-ethyl-hexanamide ((*S*)-14)**

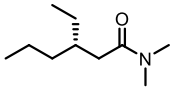

(*S*)-14

In a flame-dried Schlenk tube equipped with septum and magnetic stirring bar, $CuBr{\cdot}SMe_2$ (1.64 mg, 0.008 mmol, 5 mol%) and ligand ($R$,$S_{Fe}$)-**L1** (6.15 mg, 0.0096 mmol, 6 mol%) were dissolved in 1.6 mL DCM and stirred under nitrogen atmosphere for 20 min. The substrate **(*Z*)-13** (0.16 mmol) was added at once. After stirring for 5 min. at RT the reaction mixture was cooled down to −78 °C, followed by addition of $BF_3{\cdot}Et_2O$ (40 $\mu$L, 0.32 mmol) or TMSOTf (58 $\mu$L, 0.32 mmol). After 20 min., EtMgBr was added by hand in about 1 min. After stirring for 18 h, the reaction was quenched with MeOH followed by addition of saturated aqueous $NH_4Cl$ solution and warming up to RT. The reaction mixture was extracted with DCM (10 mL × 3). Combined organic phases were dried over $MgSO_4$, filtered and solvents were evaporated on a rotary evaporator. Product **(*S*)-14** was obtained as a colorless oil after column chromatography ($SiO_2$, pentane:$Et_2O$ = 1:1). $^1$H NMR ($CDCl_3$, 400 MHz): $\delta$ 3.00 (s, 3H, NC$H_3$), 2.93 (s, 3H, NC$H_3$), 2.21 (dd, $J$ = 15.1, 7.1 Hz, 1H, C$H$HCO), 2.20 (dd, $J$ = 15.1, 6.7 Hz, 1H, CH$H$CO), 1.91-1.81 (m, 1H, C$H$CH$_2$), 1.36-1.21 (m, 5H, C$H_2$CH$_3$, CH$_2$C$H_2$CH$_3$), 1.24-1.18 (m, 1H, CH$H$CH$_3$), 0.87 (d, $J$ = 7.0 Hz, 3H, C$H_3$CH), 0.85 (t, $J$ = 7.5 Hz, 3H, C$H_3$CH$_2$). HPLC: Chiracel-OBH, *n*-heptane/*i*-PrOH 95:5, 0.5 mL/min, 40 °C, detection at 210 nm. Retention time (min): 10.4 (major) and 11.5 (minor).

**(*R*)-*N*,*N*-Dimethyl-3-methyl-hexanamide ((*R*)-15)**

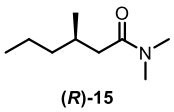

(*R*)-15

In a flame-dried Schlenk tube equipped with septum and magnetic stirring bar, $CuBr{\cdot}SMe_2$ (2.06 mg, 0.01 mmol, 5 mol%) and ligand ($R$,$S_{Fe}$)-**L1** (7.68 mg, 0.012 mmol, 6 mol%) were dissolved in 2.0 mL DCM and stirred under nitrogen atmosphere for 20 min. The substrate **(*E*)-13** (0.2 mmol) was added at once. After stirring for 5 min. at RT the reaction mixture was cooled down to −78 °C, followed by addition of $BF_3{\cdot}Et_2O$ (50 $\mu$L, 0.4 mmol) or TMSOTf (72 $\mu$L, 0.4 mmol). After 20 min., MeMgBr was added by hand in about 1 min. After stirring for 18 h, the reaction was quenched with MeOH followed by addition of saturated aqueous $NH_4Cl$ solution and warming up to RT. The reaction mixture was extracted with DCM (10 mL × 3). Combined organic phases were dried over $MgSO_4$, filtered and solvents were evaporated on a rotary evaporator. Product **(*R*)-15** was obtained as a colorless oil after column chromatography ($SiO_2$, pentane:$Et_2O$ = 1:1). $^1$H NMR ($CDCl_3$, 400 MHz): $\delta$ 3.00 (s, 3H, NC$H_3$), 2.95 (s, 3H, NC$H_3$), 2.29 (dd, $J$ = 14.6, 5.8 Hz, 1H, C$H$HCO), 2.12 (dd, $J$ = 14.6, 8.1 Hz, 1H, CH$H$CO), 2.05-1.97 (m, 1H, C$H$CH$_2$), 1.43-1.24 (m, 3H, C$H_2$CH$_3$, C$H$HCH$_2$CH$_3$), 1.19-

1.10 (m, 1H, CH*H*CH$_2$CH$_3$), 0.93 (d, *J* = 6.6 Hz, 3H, C*H*$_3$CH), 0.89 (t, *J* = 7.0 Hz, 3H, C*H*$_3$CH$_2$). $^{13}$C NMR ($CDCl_3$, 100 MHz): $\delta$ 172.9, 40.8, 39.5, 37.6, 35.5, 30.2, 20.3, 20.0, 14.4. HRMS (ESI+, m/Z): calcd. for $C_9H_{20}NO$ $[M+H]^+$: 158.1539, found: 158.1538. HPLC: Chiracel-OBH, *n*-heptane/*i*-PrOH 90:10, 0.5 mL/min, 40 °C, detection at 206 nm. Retention time (min): 9.1 (minor) and 10.2 (major).

**(*S*)-*N*,*N*-Dimethyl-3-methyl-hexanamide ((*S*)-15)**

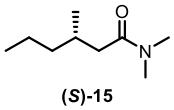

(*S*)-15

In a flame-dried Schlenk tube equipped with septum and magnetic stirring bar, CuBr·$SMe_2$ (1.64 mg, 0.008 mmol, 5 mol%) and ligand (*R*,*S*$_{Fe}$)-**L1** (6.15 mg, 0.0096 mmol, 6 mol%) were dissolved in 1.6 mL DCM and stirred under nitrogen atmosphere for 20 min. The substrate **(*Z*)-13** (0.16 mmol) was added at once. After stirring for 5 min. at RT the reaction mixture was cooled down to −78 °C, followed by addition of $BF_3$·$Et_2O$ (40 $\mu$L, 0.32 mmol) or TMSOTf (58 $\mu$L, 0.32 mmol). After 20 min., MeMgBr was added by hand in about 1 min. After stirring for 18 h, the reaction was quenched with MeOH followed by addition of saturated aqueous $NH_4Cl$ solution and warming up to RT. The reaction mixture was extracted with DCM (10 mL × 3). Combined organic phases were dried over $MgSO_4$, filtered and solvents were evaporated on a rotary evaporator. Product **(*S*)-15** was obtained as a colorless oil after column chromatography ($SiO_2$, pentane:$Et_2O$ = 1:1). $^1$H NMR ($CDCl_3$, 400 MHz): $\delta$ 3.00 (s, 3H, NC*H*$_3$), 2.95 (s, 3H, NC*H*$_3$), 2.29 (dd, *J* = 14.6, 5.8 Hz, 1H, C*H*HCO), 2.12 (dd, *J* = 14.6, 8.1 Hz, 1H, CH*H*CO), 2.05-1.97 (m, 1H, C*H*CH$_2$), 1.43-1.24 (m, 3H, C*H*$_2$CH$_3$, C*H*HCH$_2$CH$_3$), 1.19-1.10 (m, 1H, CH*H*CH$_2$CH$_3$), 0.93 (d, *J* = 6.6 Hz, 3H, C*H*$_3$CH), 0.89 (t, *J* = 7.0 Hz, 3H, C*H*$_3$CH$_2$). HPLC: Chiracel-OBH, *n*-heptane/*i*-PrOH 90:10, 0.5 mL/min, 40 °C, detection at 206 nm. Retention time (min): 9.1 (major) and 10.2 (minor).

**TMS-amide complex**

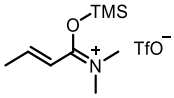


TMSOTf (16 $\mu$L, 0.088 mmol) was added to a solution of carboxamide **7** (10 mg, 0.088 mmol) in $CD_2Cl_2$ (0.6 mL) in a dry NMR tube at −78 °C under $N_2$ atmosphere, leading to instantaneous formation of a new species which was immediately measured by NMR spectroscopy at −80 °C. $^1$H NMR ($CD_2Cl_2$, 400 MHz): $\delta$ 6.81 (dq, *J* = 15.5, 6.9 Hz, 1H), 6.41 (dd, *J* = 15.5, 1.5 Hz, 1H), 3.37 (s, 3H), 3.25 (s, 3H), 2.05-2.00 (m, 3H), 0.36 (s, 9H). $^{13}$C NMR ($CD_2Cl_2$, 100 MHz): $\delta$ 167.2, 152.5, 117.7, 40.4, 38.8, 19.4, 0.2. $^{29}$Si NMR ($CD_2Cl_2$, 79.5 MHz): $\delta$ 38.4. $^{19}$F NMR ($CD_2Cl_2$, 376.6 MHz): $\delta$ −79.17.

**$BF_3$-amide complex**

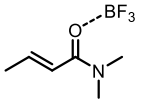

$BF_3{\cdot}Et_2O$ ( 10 $\mu$L, 0.08 mmol) was added to a solution of carboxamide **7** (10 mg, 0.088 mmol) in $CD_2Cl_2$ (0.6 mL) in a dry NMR tube at −78 °C under $N_2$ atmosphere, leading to instantaneous formation of a new species which was immediately measured by NMR spectroscopy at −80 °C. $^1$H NMR ($CD_2Cl_2$, 400 MHz): $\delta$ 13.55 (s, 1H), 6.78 (dq, $J$ = 13.6, 6.8 Hz, 1H), 6.23 (d, $J$ = 15.9, 1H), 3.30 (s, 3H), 3.22 (s, 3H), 2.00 (d, $J$ = 6.8 Hz, 3H) (Major species). $^{13}$C NMR ($CD_2Cl_2$, 100 MHz): $\delta$ 169.7, 149.0, 117.6, 41.0, 38.7, 19.9, 14.6 (Major species). $^{11}$B NMR ($CD_2Cl_2$, 100 MHz): $\delta$ −0.26, −0.74, −1.22, −1.28. $^{19}$F NMR ($CD_2Cl_2$, 100 MHz): $\delta$ −146.82 ($^{19}$F-$^{10}$B), −146.88 ($^{19}$F-$^{11}$B).

**Silyl enolate**

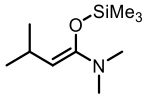


In a flame-dried Schlenk tube equipped with septum and magnetic stirring bar, CuBr-($R$,$S_{Fe}$)-**L1** complex (5.53 mg, 0.0075 mmol, 5 mol%) and amide **7** (17 mg, 0.15 mmol) were dissolved in $CD_2Cl_2$ (1.5 mL) and stirred under nitrogen atmosphere. After stirring at room temperature for 5 min., the reaction mixture was cooled to −60 °C and TMSOTf (52 $\mu$L, 0.30 mmol) was added. After 15 min., MeMgBr (100 $\mu$L, 0.30 mmol, 3.0 M in $Et_2O$) was added. After stirring at −60 °C for 18 h, the mixture was transferred to a NMR tube followed by measurement at −80 °C. $^1$H NMR ($CD_2Cl_2$, 400 MHz): $\delta$ 3.39 (d, $J$ = 9.4 Hz, 1H), 2.42-2.32 (m, 1H), 2.33 (s, 6H), 0.81 (d, $J$ = 6.7 Hz, 6H), 0.08 (s, 9H). $^{13}$C NMR ($CD_2Cl_2$, 100 MHz): $\delta$ 152.1, 95.7, 40.4, 25.3, 24.5, −0.4. $^{29}$Si NMR ($CD_2Cl_2$, 79.5 MHz): $\delta$ 19.3.

**Boron enolate**

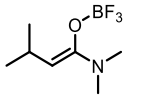


In a flame-dried Schlenk tube equipped with septum and magnetic stirring bar, CuBr-($R$,$S_{Fe}$)-**L1** complex (5.53 mg, 0.0075 mmol, 5 mol%) and amide **7** (17 mg, 0.15 mmol) were dissolved in $CD_2Cl_2$ (1.5 mL) and stirred under nitrogen atmosphere. After stirring at room temperature for 5 min., the reaction mixture was cooled to −60 °C and $BF_3{\cdot}Et_2O$ (37 $\mu$L, 0.30 mmol) was added. After 15 min., MeMgBr (100 $\mu$L, 0.30 mmol, 3.0 M in $Et_2O$) was added. After stirring at −60 °C for 18 h, the mixture was transferred to a NMR tube, cooled and measured by NMR spectroscopy at −80 °C. $^1$H NMR ($CD_2Cl_2$, 400 MHz): $\delta$ 4.78 (d, $J$ = 10.3 Hz, 1H), 2.66 (s, 6H), 2.50-2.42 (m, 1H), 0.89 (d, $J$ = 6.6 Hz, 6H). $^{13}$C NMR ($CD_2Cl_2$, 100 MHz): $\delta$ 132.7, 111.6, 44.5, 25.5, 22.7.

**Magnesium enolate**

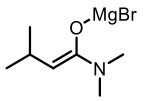


A 3.0 M MeMgBr solution in $Et_2O$ (67 $\mu$L, 0.2 mmol) was added to a solution of amide **7** (12 mg, 0.10 mmol) in $CD_2Cl_2$ (0.6 mL) in a dry NMR tube under $N_2$ atmosphere. After 18 h the mixture was measured by NMR spectroscopy at −80 °C. $^1$H NMR ($CD_2Cl_2$, 400 MHz): $\delta$ 3.97

(d, $J$ = 8.7 Hz, 1H), 2.41 (s, 6H), 2.38-2.27 (m, 1H), 0.84 (d, $J$ = 6.6 Hz, 6H). $^{13}$C NMR ($CD_2Cl_2$, 100 MHz): $\delta$ 129.7, 110.0, 40.4, 26.9, 24.1.

## 3.5 References


[1] A. Alexakis, N. Krause, S. Woodward, *Copper-Catalysed Asymmetric Synthesis*, Wiley-VCH, Weinheim, Germany, **2014**.

[2] S. R. Harutyunyan, *Progress in Enantioselective Cu(I)-catalyzed Formation of Stereogenic Centers*, Springer, Heidelberg, **2015**.

[3] T. Jerphagnon, M. G. Pizzuti, A. J. Minnaard, B. L. Feringa, *Chem. Soc. Rev.* **2009**, *38*, 1039–1075.

[4] S. R. Krauss, S. G. Smith, *J. Am. Chem. Soc.* **1981**, *103*, 141–148.

[5] J. Canisius, A. Gerold, N. Krause, *Angew. Chem. Int. Ed.* **1999**, *38*, 1644–1645.

[6] D. E. Frantz, D. A. Singleton, J. P. Snyder, *J. Am. Chem. Soc.* **1997**, *119*, 3383–3384.

[7] S. Mori, M. Uerdingen, N. Krause, K. Morokuma, *Angew. Chem. Int. Ed.* **2005**, *44*, 4715–4719.

[8] K. Nilson, C. Anderson, A. Ullenius, A. Gerold, N. Krause, *Chem. Eur. J.* **1998**, *4*, 2051–2058.

[9] C. P. Casey, M. Cesa, *J. Am. Chem. Soc.* **1979**, *101*, 4236–4244.

[10] B. Christenson, T. Olsson, C. Ullenius, *Tetrahedron* **1989**, *45*, 523–534.

[11] S. H. Bertz, R. A. Smith, *J. Am. Chem. Soc.* **1989**, *111*, 8276–8277.

[12] S. H. Bertz,; M. K. Carlin, D. A. Deadwyler, M. Murphy, C. A. Ogle, P. H. A. Seagle, *J. Am. Chem. Soc.* **2002**, *124*, 13650–13651.

[13] K. Nilsson, C. Ullenius, N. Krause, *J. Am. Chem. Soc.* **1996**, *118*, 4194–4195.

[14] N. Krause, R. Wagner, A. Gerold, *J. Am. Chem. Soc.* **1994**, *116*, 381–382.

[15] M. Yamanaka, E. Nakamura, *J. Am. Chem. Soc.* **2004**, *126*, 6287–6293.

[16] M. Yamanaka, E. Nakamura, *J. Am. Chem. Soc.* **2005**, *127*, 4697–4706.

[17] S. R. Harutyunyan, F. López, W. R. Browne, A. Correa, D. Peña, R. Badorrey, A. Meetsma, A. J. Minnaard, B. L. Feringa, *J. Am. Chem. Soc.* **2006**, *128*, 9103–9118.

[18] F. López, S. R. Harutyunyan, A. J. Minnaard, B. L. Feringa, *Angew. Chem. Int. Ed.* **2005**, *44*, 2752–2756.

[19] N. Yoshikai, E. Nakamura, *Chem. Rev.* **2012**, *112*, 2339–2372.

[20] E. J. Corey, N. W. Boaz, *Tetrahedron Lett.* **1985**, *26*, 6015–6018.

[21] E. J. Corey, N. W. Boaz, *Tetrahedron Lett.* **1985**, *26*, 6019–6022.

[22] A. Alexakis, J. Berlan, Y. Besace, *Tetrahedron Lett.* **1986**, *27*, 1047–1050.

[23] S. Matsuzawa, Y. Horiguchi, E. Nakamura, I. Kuwajima, *Tetrahedron* **1989**, *45*, 349–362.

[24] S. H. Bertz, G. Miao, B. E. Rossiter, J. P. Snyder, *J. Am. Chem. Soc.* **1995**, *117*, 11023–11024.

[25] D. E. Frantz, D. A. Singleton, *J. Am. Chem. Soc.* **2000**, *122*, 3288–3295.

[26] Y. Yamamoto, S. Yamamoto, H. Yatagai, Y. Ishihara, K. Maruyama, *J. Org. Chem.* **1982**, *47*, 119–126.

[27] B. H. Lipshutz, E. L. Ellsworth, S. H. Dimock, *J. Am. Chem. Soc.* **1990**, *112*, 5869–5871.

[28] E. Nakamura, M. Yamanaka, S. Mori, *J. Am. Chem. Soc.* **2000**, *122*, 1826–1827.

[29] K. Biswas, S. Woodward, *Tetrahedron: Asymmetry* **2008**, *19*, 1702–1708.